ADVANCED MATERIALS INTERFACES
www.advmatinterfaces.de

Managing Energy Loss in Inorganic Lead Halide Perovskites Solar Cells

*Chongming Liu, Qingsen Zeng, and Bai Yang**

Though the cesium-based inorganic perovskite solar cells (IPSCs) have developed rapidly in recent two years, the power conversion efficiency (PCE) is still far away from the Shockley–Queisser limit due to the large open-circuit voltage (V_{oc}) deficit, which results from the large energy loss (E_{loss}). Large E_{loss} has been a major obstacle for further efficiency improvement of IPSCs. In this review, the authors, for the first time, focus on investigating the E_{loss} of IPSCs and start from discussing the essence and origin of the E_{loss}. Then, the reported efficient methods for reducing the band tails and energy disorder are systematically summarized and reviewed, including crystallization optimization, defect passivation, and interface engineering. Finally, the authors offer an overall perspective on managing E_{loss} in IPSCs and point out the possible ways to reduce the E_{loss} and promote the efficiency. This review provides a basic understanding of E_{loss} and may inspire new designs or more impactful methods for further minimizing the E_{loss} of IPSCs.

1. Introduction

Since the first report of lead halide perovskite solar cells (PSCs) in 2009,[1] the power conversion efficiency (PCE) of single-junction PSCs has reached 24.2%.[2] The great success originates from the excellent photoelectronic properties of perovskite materials, including high absorption coefficient,[3] low trap state density,[4,5] high carrier mobility, long carrier lifetimes,[6] and diffusion length.[4,7] In the next stage, it is urgent to overcome the problem of device stability. Stable perovskite material is one of the keys. Inorganic cesium lead halide perovskite have attracted much attentions and developed dramatically in the past two years, due to their better stability in stress conditions, especially the outstanding thermal stability.[8] In inorganic cesium lead halide perovskites, $CsPbI_3$ is the most suitable for photovoltaic applications due to the relatively narrow bandgap of 1.73 eV. Generally, bulk $CsPbI_3$ suffers from thermodynamic phase instability, and the black phase of the α-$CsPbI_3$ spontaneously transforms to the undesired yellow δ-phase (with bandgap of 2.82 eV) under ambient air condition when the temperature reduces to room temperature.[9] Even though, many strategies have been developed to achieve the stable $CsPbI_3$ materials and thus stable operating devices, including reducing the grain size,[10] doping ions,[11] surface modification,[12] and encapsulation.[13] Besides, mixed-halide $CsPbI_2Br$ perovskite formed by partial substitution of the iodide with bromide is another optimal candidate as an photoactive layer due to its much more stable phase.[14] In addition, $CsPbI_2Br$, with a constant energy barrier for ion migration in dark and under light illumination, exhibit excellent photostability and suppressed light-induced phase separation compared to the MA-based hybrid composites.[15] Apart from the widely explored $CsPbI_3$ and $CsPbI_2Br$, $CsPbBr_2I$ and $CsPbBr_3$ with much broader bandgaps are also promising for preparing stable perovskite solar cells, and have made great progress in recent two years.[16,17]

Since the introduction of inorganic perovskite solar cells (IPSCs) in 2015,[18] many groups have achieved the efficiencies over 16% based on $CsPbI_2Br$ and $CsPbI_3$. So far, the highest PCE 17.06% is achieved by the Zhao group through treating $CsPbI_3$ films with phenyltrimethylammonium bromide (PTABr), which acts as a bifunctional stabilization to realize gradient Br doping and surface passivation.[12] Even though, the PCE is still far away from their theoretical limited efficiency,[19] and there is great potential for further improvement.

As we all know, PCE is the product of short current density (J_{sc}), fill factor (FF), and open circuit voltage (V_{oc}), and can be expressed by this equation: $\mathrm{PCE} = J_{sc} \times FF \times V_{oc}/P_s$, where the P_s is irradiance light power. Maximizing the three parameters simultaneously is the way to the Shockley–Queisser (SQ) limits. The tabulated values of the SQ limit for single junction solar cells have been calculated by Rühle.[19] Currently, the percentages of the J_{sc} and FF versus their SQ limits are above 95% and 85% respectively. But the percentage of V_{oc} versus the SQ limit is just ≈80% accounting for the low percentage of PCE SQ limit (≈65%). Take the $CsPbI_2Br$ IPSCs as an example, the bandgap of $CsPbI_2Br$ is ≈1.92 eV. The corresponding SQ limits for J_{sc}, V_{oc}, and PCE are 16.5 mA cm^{-2}, 1.6 V, and 24.3%, respectively. Up to now, the most highest PCE of $CsPbI_2Br$ IPSCs with

---

C. Liu, Dr. Q. Zeng, Prof. B. Yang
State Key Laboratory of Supramolecular Structure and Materials
College of Chemistry
Jilin University
Changchun 130012, P. R. China
E-mail: byangchem@jlu.edu.cn

Prof. B. Yang
State Key Laboratory of Applied Optics
Changchun Institute of Optics Fine Mechanics and Physics
Chinese Academy of Sciences
Changchun 130033, P. R. China

The ORCID identification number(s) for the author(s) of this article can be found under https://doi.org/10.1002/admi.201901136.

DOI: 10.1002/admi.201901136

bandgap 1.92 eV, reported by Cao group, is 16.2% with a V_{oc} of 1.30 V and J_{sc} of 15.3 mA cm^{-2}.[20] Obviously, the V_{oc} is only 81% of the SQ limit, leaving much room for further improvement. Therefore, to achieve higher PCE, it is critical to improve the V_{oc} through reducing the energy loss (E_{loss}).

This paper gives an overview on managing the E_{loss} in IPSCs. We first describe the essence of E_{loss} and analyze the origin of E_{loss} in details. Then, we summarize the effective strategies for minimizing the E_{loss} in IPSCs, including the improvement of film quality, defect passivation and interface engineering. This paper will enlighten researchers to further promote the efficiency of IPSCs by minimizing the E_{loss}.

2. Determination of V_{oc} and Origin of E_{loss}

Under dark condition, a thermal equilibrium is formed in a photovoltaic device, and the uniform Fermi level is aligned throughout the device as presented **Figure 1**a. Once the sunlight strikes solar cell, the thermal equilibrium is broken. The received energy can be divided into two parts, excitions generation and heat production. The excitions will dissociate into free electrons and holes with opposite polarity. At the same time, the Fermi level splits into two quasi Femi levels, the electron quasi Fermi level (E_{Fn}) and hole quasi Fermi level (E_{Fp}), as shown in Figure 1b.[21] The difference between E_{Fn} and E_{Fp} determines the value of V_{oc}. The relationship between theoretical limited V_{oc} ($V_{\text{oc-SQ}}$), V_{oc}, E_{Fn}, and E_{Fp} can be expressed as Equation (1)[19,22,23]

$$V_{\text{oc-SQ}} > V_{\text{oc}} = \frac{1}{e}\left|E_{\text{Fn}} - E_{\text{Fp}}\right| \tag{1}$$

The E_{Fn} and E_{Fp} are affected by the occupation of the available electronic states, which are occupied by photogenerated charge carriers in the whole device.[24] The band tails and energy disorder can cause E_{loss} and are harmful to the V_{oc}, as exhibited in Figure 1c. The band tails or energy disorder both in the perovskite active layer and interfacial transport layer can act as available electronic states, which can also be occupied by carriers. These unexpected electronic states cause energy loss of excited charge carriers and decrease the difference between E_{Fn} and E_{Fp}, thus leading to reduced V_{oc}.

The relationship between E_{loss} and V_{oc} can be described as Equation (2)

$$E_{\text{loss}} = E_{\text{g}} - eV_{\text{oc}} \tag{2}$$

where E_{g} is the bandgap of active layer and e is the electron charge. Take the unavoidable carrier recombination loss into account, the $V_{\text{oc-SQ}}$ is always lower than the value of E_{g}/e.[19] The energy disorder and band tail are another part of carrier loss, making the V_{oc} lower than $V_{\text{oc-SQ}}$. These two parts of carrier loss cause the E_{loss}. Thus, in order to minimize the E_{loss}, what we can do is to reduce the energy disorder and band tail in device.

We have summarized the E_{loss} and V_{oc} versus bandgaps of all the reported IPSCs as shown in **Figure 2**a,b, and the detail performance parameters are listed in **Tables 1–5**. The I-rich $CsPbI_2Br$ and $CsPbI_3$ IPSCs are widely studied due to their relatively lower bandgaps. The value of E_{loss} is highly dependent on the bandgaps of perovskites, and tends to be enlarged with increased bandgaps. Compared with the Br-rich ($CsPbIBr_2$ and $CsPbBr_3$) IPSCs, the E_{loss} of $CsPbI_2Br$ and $CsPbI_3$ is relatively lower and lies in the range 0.65–0.85 eV and 0.60–0.80 eV, respectively. One of $CsPbBr_3$ devices achieved the highest V_{oc} of 1.594 V in PSCs through Sm^{3+} doping. But, due to the large bandgap of 2.3 eV for $CsPbBr_3$, the E_{loss} still reaches 0.706 eV.[25] Only few devices achieve the E_{loss} lower than 0.55 eV. The lowest E_{loss} 0.45 eV in IPSCs was achieved by a polymer-passivated $CsPbI_3$ QDs device, but the only fly in the ointment is the moderate PCE of 12.55% because of the small J_{sc} of 12.39 mA cm^{-2}.[26]

Chongming Liu is a master student at the State Key Lab of Supramolecular Structure and Materials under the supervision of Prof. Bai Yang, majoring in polymer chemistry and physics. He is interested in the synthesis of inorganic perovskite quantum dots as well as their optoelectronic applications.

Qingsen Zeng is a postdoctor at the State Key Lab of Supramolecular Structure and Materials. He received his Ph.D. in polymer physics and Chemistry in 2019 under the supervision of Prof. Bai Yang. He is interested in organic polymer– and inorganic nanocrystal–based photoelectronic materials, and now focuses on exploring new procedure to synthesize the stable $CsPbX_3$ perovskite nanocrystals and optimizing their performance in polymer-based hybrid solar cells and light-emitting devices.

Bai Yang is a professor of chemistry at the State Key Lab of Supramolecular Structure and Materials in the College of Chemistry, Jilin University. He received his Ph.D. in polymer physics and chemistry in 1991 under the supervision of Prof. Jiacong Shen at Jilin University. His current research interests include carbon-based nanodots (carbonized polymer dots and graphene quantum dots), polymer-/nanocrystal-based high-performance optical and photoelectric materials, and multiscale ordered polymeric microstructures for photonic responsive materials.

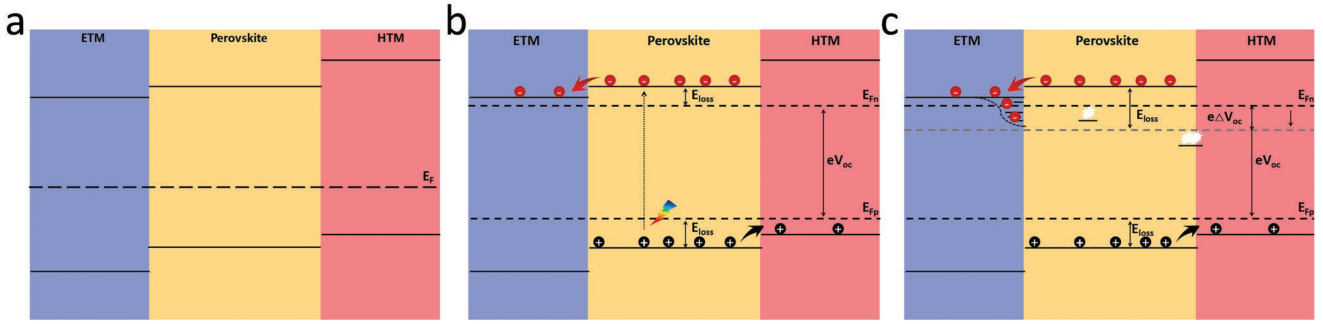

Figure 1. a) Thermal equilibrium of IPSC Fermi level under dark condition. b) Fermi level splits into quasi-Fermi levels under illumination condition. c) E_{loss} of IPSC in the actual condition.

In addition, we note that the ion-doped IPSCs and quantum dots (QDs) IPSCs exhibit surprising high V_{oc} with low E_{loss}. We will discuss these interesting IPSCs in details in the following part. We also plot the PCE versus E_{loss} in Figure 2c, and we can draw a conclusion that high-efficiency IPSCs devices always show relatively low E_{loss}. In comparison with IPSCs, the lowest E_{loss} of organic-inorganic hybrid perovskite solar cells (HPSCs) has been down to only 0.35 eV through managing the band tails of the device, which accounts for the high PCE of 23.3%.[27] Therefore, there is still much room for the E_{loss} reduction through eliminating the band tails and energy disorder.

3. Strategies of Minimizing E_{loss}

As discussed above, the band tails caused by the energy disorder in perovskites, transport layers and their interfaces are responsible for the E_{loss}. Therefore, the reduction of E_{loss} can be achieved through reducing the band tails and energy disorder of the device. Here, we summarize efficient strategies of minimizing E_{loss} in IPSCs from three aspects, including improvement of the perovskite film quality, defect passivation and interface engineering.

3.1. Improvement of the Perovskite Film Quality

Theoretical calculations have turned out that the grain boundaries of perovskites are benign.[28,29] Nevertheless, many experimental works have observed the grain boundaries greatly affect the photoelectronic properties of perovskites.[30] For example, carrier diffusion lengths in $MAPbI_3$ microcrystal is on the order of several hundred nanometers, however, $MAPbI_3$ single crystal shows the diffusion length exceeding 175 µm.[4] Defects like to inhabit at the grain boundaries[31] and constitute a major pathway for E_{loss}. Therefore, a high-quality perovskite film with larger grain size, less grain boundaries, and pin holes is necessary for the high-performance IPSCs. Compared to MA- and FA-based hybrid perovskites, the control on film morphology of solution-processed cesium-based inorganic perovskites is relatively difficult, especially for the Br-rich composition owing to the inferior solubility of bromide species.[32] Therefore, most primary works focus on the optimizations of morphology and crystallinity of inorganic perovskite films. During the process of the film formation, the selected solvents, annealing procedures, and additives all have great impacts on the final film quality.

3.1.1. Solvent Engineering

One-step spin-coating method is the usual way to deposit perovskite films. Normally, the DMF/DMSO mixed solution is used to dissolve the precursors. The content of DMSO plays an important role in the crystallization and quality of the film. The major works on solvent engineering are conducted for $CsPbI_2Br$ IPSCs because the CsBr precursor is hard to dissolve in DMF.[33]

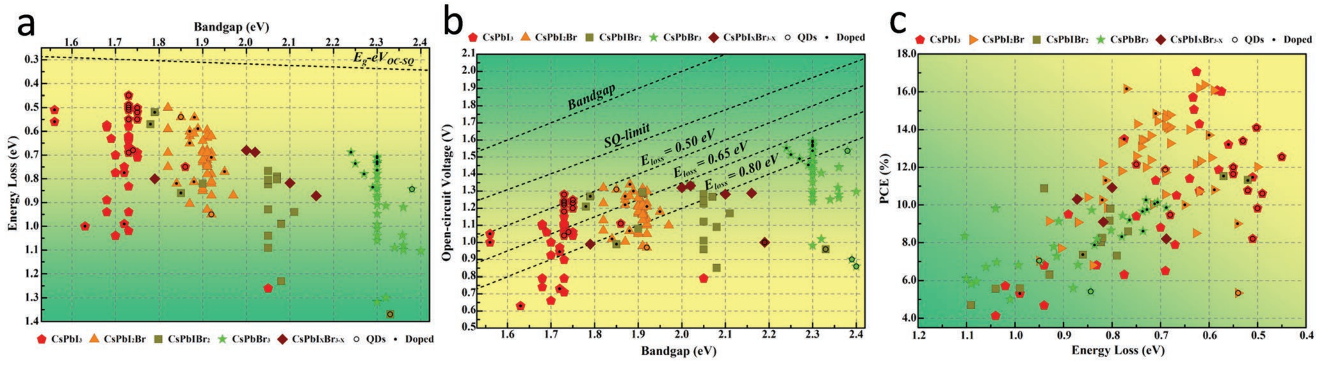

Figure 2. The plots of a) E_{loss} versus bandgap, b) V_{oc} versus bandgap, c) PCE versus E_{loss} in all the reported inorganic perovskite solar cells.

Table 1. Photovoltaic parameters and E_{loss} of $CsPbI_3$ IPSCs.

Cell structure	J_{sc} [mA cm^{-2}]	V_{oc} [V]	FF [%]	PCE [%]	Highest V_{oc} [V]	Bandgap [eV]	E_{loss} [eV]	Ref.
FTO/TiO_2/PTABr-$CsPbI_3$/Spiro/Ag	19.15	1.104	80.6	17.06	1.104	1.73	0.626	[12]
ITO/PEDOT:PSS/$CsPbI_3$/PCBM/Al	15	1.06	41	6.5	1.06	1.75	0.69	[77]
FTO/SnO_2/$CsPbI_3$/Spiro/Ag	13	1	68	8.8	1	1.7	0.7	[78]
ITO/SnO_2/$CsPbI_3$/Spiro/Au	18.41	1.08	79.32	15.71	1.097	1.73	0.633	[13]
FTO/TiO_2/$CsPbI_3$ QDs/Spiro/MoO_x/Al	13.47	1.23	65	10.77	1.23	1.75	0.52	[10]
FTO/TiO_2/μGR-$CsPbI_3$ QDs/PTAA/Au	13.59	1.18	72.6	11.64	1.18	1.73	0.55	[79]
FTO/TiO_2/$CsPbI_3$/Spiro/Ag	11.92	0.66	52.47	4.13	0.66	1.7	1.04	[80]
ITO/TiO_2/$CsPbI_3$/P3HT/Au	13.8	1.063	71.6	10.5	1.063	1.73	0.667	[81]
FTO/m-TiO_2/$CsPbI_3$/C	18.5	0.79	65	9.5	0.79	1.68	0.89	[82]
FTO/TiO_2/$CsPbI_3$/P3HT/Au	16.53	1.04	65.7	11.3	1.04	1.75	0.71	[83]
FTO/TiO_2/$CsPbI_3$-PEAI/PTAA/Au	18.95	1.059	75.1	15.07	1.059	1.69	0.631	[84]
FTO/TiO_2/$CsPbI_3$:$Cl_{0.03}$/PTAA/Au	19.58	1.084	75.7	16.07	1.097	1.68	0.583	[85]
FTO/TiO_2/AX-$CsPbI_3$ QDs/Spiro/MoO_x/Al	14.37	1.2	78	13.4	1.22	1.75	0.53	[75]
FTO/TiO_2/$CsPbI_3$/Spiro/Au	14.88	1.11	65	10.74	1.11	1.73	0.62	[52]
ITO/PTAA/$CsPb(I_{0.98}Cl_{0.02})_3$/PCBM/$C_{60}$/BCP/Al	14.9	1.08	70	11.4	1.09	1.73	0.64	[86]
FTO/TiO_2/$CsPbI_3$·0.05$DETAI_3$/P3HT/Au	12.21	1.06	61	7.89	1.06	1.73	0.67	[87]
FTO/TiO_2/m-TiO_2/$CsSn_{0.6}Pb_{0.4}I_3$QDs/Spiro/Au	10.13	0.63	0.46	2.9	0.63	1.63	1	[88]
FTO/TiO_2/$CsPb_{0.96}Bi_{0.04}I_3$/CuI/Au	18.76	0.97	72.59	13.21	1	1.56	0.56	[11]
PET-ITO/TiO_2/$CsPb_{0.96}Bi_{0.04}I_3$/Spiro/Au	15.11	1.05	72.32	11.47	1.05	1.56	0.51	[43]
MgF_2/FTO/TiO_2/m-TiO_2/$CsPb_{0.95}Ca_{0.05}I_3$/P3HT/Au	17.9	0.945	80	13.5	0.945	1.72	0.775	[89]
FTO/TiO_2/m-TiO_2/m-Al_2O_3/$CsPb_{0.96}Sb_{0.04}I_3$/C	14.65	0.73	50	5.31	0.73	1.72	0.99	[90]
FTO/TiO_2/$CsPbI_3$·0.05Eu/Spiro/Au	11.1	0.898	68	6.8	0.898	1.73	0.832	[91]
FTO/TiO_2/$CsPbI_3$ QDs/PTB7/MoO_3/Ag	12.39	1.27	80	12.55	1.28	1.73	0.45	[26]
FTO/TiO_2/$CsPbI_3$ QDs/PTB7-Th/MoO_3/Ag	11.05	1.24	78	10.6	1.24	1.73	0.49	
FTO/TiO_2/$CsPbI_3$ QDs/P3HT/MoO_3/Ag	10.91	1.23	73	9.82	1.23	1.73	0.5	
FTO/TiO_2/$CsPbI_3$ QDs/Spiro/MoO_3/Ag	9.84	1.22	68	8.2	1.22	1.73	0.51	
N-GQD EDS/FTO/TiO_2/$CsPbI_3$/PTAA/Au	19.15	1.106	75.6	16.02	1.106	1.68	0.574	[92]
FTO/TiO_2/m-TiO_2/$CsPbI_3$/P3HT/MoO_3/Au	10.48	0.74	61	4.68	0.74	1.68	0.94	[93]
FTO/TiO_2/$CsPbI_3$:0.025$EDAI_2$/Spiro/Ag	14.53	1.15	71	11.86	1.15	1.73	0.58	[41]
ITO/PEDOT:PSS/$CsPbI_3$/$PC_{71}BM$/Ag	12.83	0.875	56.21	6.3	0.925	1.7	0.775	[94]
FTO/TiO_2/$CsPbI_3$/P3HT/Ag	12.06	0.79	72	6.79	0.79	1.73	0.94	[95]
FTO/TiO_2/$CsPbI_3$/P3HT/Ag	12.06	0.71	67	5.71	0.71	1.73	1.02	[96]
FTO/TiO_2/$CsPbI_3$/Spiro/Ag	18.5	1.11	69.6	14.3	1.11	1.73	0.62	[54]
ITO/PEDOT:PSS/$CsPbI_3$/PCBM/Al	0.26	0.79	45	0.09	0.79	2.05	1.26	[97]
ITO/Ca/C_{60}/$CsPbI_3$/TAPC/TAPC:MoO_3/Ag	17.4	0.97	56	9.4	0.97	1.72	0.75	[98]
FTO/TiO_2/$CsPbI_3$ QDs/Spiro/MoO_x/Al		1.2		≈12	1.2	1.75	0.55	[99]
FTO/TiO_2/$CsPbI_3$ QDs/Spiro/Au	14.8	1.11	74	12.15	1.11	1.86	0.75	[73]
FTO/TiO_2/$CsPbI_3$ QDs/Spiro/MoO_3/Ag	12.24	1.06	73	9.47	1.06	1.74	0.68	[100]
FTO/TiO_2/CsAc-$CsPbI_3$ QDs/PTAA/MoO_x/Ag	14.96	1.248	75.6	14.1	1.248	1.75	0.502	[101]
FTO/TiO_2/$CsPbI_3$ QDs/Spiro/Au	16.98	1.04	67.2	11.87	1.04	1.73	0.69	[102]

Chen et al. studied the influence of DMSO on device performance based on an inverted planar architecture, FTO/NiMgLiO/$CsPbI_2Br$/PCBM/BCP/Ag. The introduction of DMSO in DMF not only facilitates dissolution of precursors but also serves as agents coordinating with precursor to form intermediates of colloid clusters. And during the subsequent annealing process, the residual DMSO is released gradually, promoting the crystallization and grain size of the film. As a result, a 53% increase of the V_{oc} from 0.59 to 0.96 V was realized.[32] Meng et al. introduced DMSO into CsBr/methanol precursor solution for two-step spin-coating method. The DMSO retards the early crystallization kinetics of perovskite

Table 2. Photovoltaic parameters and E_{loss} of $CsPbI_2Br$ IPSCs.

Cell structure	J_{sc} [mA cm^{-2}]	V_{oc} [V]	*FF* [%]	PCE [%]	Highest V_{oc} [V]	Bandgap [eV]	E_{loss} [eV]	Ref.
MgF_2/FTO/TiO_2/$CsPbI_2Br$/FA-$CsPbI_2Br$ QDs/PTAA/Au	15.1	1.221	80.3	14.81	1.221	1.91	0.689	[36]
FTO/TiO_2/$CsPbI_2Br$/Spiro/Au	≈14	≈1.32	≈72	13.27	1.32	2	0.68	[34]
FTO/TiO_2/$CsPbI_2Br$/Spiro/Au	12	1.23	73	10.7	1.25	1.87	0.62	[103]
FTO/TiO_2/m-TiO_2/$CsPbI_2Br$/Spiro/Ag	13.56	1.243	74.3	12.52	1.315	1.91	0.595	[32]
FTO/SnO_2/$CsPbI_2Br$/Spiro/Ag	12.58	1.256	77	12.17	1.283	1.91	0.627	
FTO/TiO_2/m-TiO_2/$CsPbI_2Br$/C	10.9	1.283	60.9	8.50	1.283	1.91	0.627	
ITO/TiO_2/$CsPbI_2Br$/Spiro/Au	16.79	1.23	77.81	16.07	1.23	1.82	0.59	[14]
FTO/SnO_2/$CsPb_{0.8}Ge_{0.2}I_2Br$/P3HT/Spiro/Au	12.15	1.27	70.1	10.8	1.3	1.889	0.589	[49]
FTO/SnO_2/$CsPb_{0.8}Ge_{0.3}I_2Br$/P3HT/Spiro/Au	10.58	1.32	64.5	9	1.34	1.881	0.541	
FTO/TiO_2/m-TiO_2/$CsPb_{0.95}Eu_{0.05}I_2Br$/Spiro/Au	14.63	1.223	76.6	13.71	1.27	1.87	0.6	[50]
FTO/TiO_2/$CsPbI_2Br$/Spiro/Au	15.33	1.22	78.7	14.78	1.22	1.9	0.68	[35]
ITO/SnO_2/ZnO/$CsPbI_2Br$/Spiro/MoO_3/Ag	15	1.23	78.8	14.6	1.23	1.92	0.69	[58]
ITO/TiO_2/$CsPbI_2Br$/P3HT/Au	13.13	1.3	70.4	12.02	1.32	1.82	0.5	[56]
FTO/TiO_2/$CsPbI_2Br$ (3D-2D-0D)/PTAA/Au	12.93	1.19	80.5	12.39	1.19	1.91	0.72	[61]
FTO/TiO_2/$CsPbI_2Br$/FA-$CsPbX_3$/FA-QDs/PTAA/Au	14.51	1.223	79.6	14.12	1.223	1.91	0.687	[63]
FTO/SnO_2/$CsPbI_2Br$/Spiro/Ag	12.41	1.293	76.9	12.34	1.293	1.91	0.617	[55]
ITO/TiO_2/$CsPbI_2Br$/Spiro/Electrode	13.98	1.17	74	12	1.17	1.9	0.73	[53]
FTO/TiO_2/$CsPbI_2Br$/$CsPbI_3$ QDs/PTAA/Au	15.25	1.204	78.7	14.45	1.204	1.91	0.706	[67]
FTO/TiO_2/$CsPbI_2Br$/PTAA/Au	14.25	1.177	80.2	13.45	1.177	1.91	0.733	
ITO/TiO_2/$CsPbI_2Br$/PTAA/Au	14.55	1.227	78.7	14.05	1.227	1.91	0.683	[104]
FTO/TiO_2-PCBM/$CsPbI_2Br$/Au	15.4	1.1	72	12.2	1.1	1.92	0.82	[105]
ITO/SnO_2/$CsPbI_2Br$/Spiro/Au	15.66	1.23	73.37	14.15	1.23	1.91	0.68	[42]
FTO/TiO_2/$Cs_{0.925}K_{0.075}PbI_2Br$/Spiro/Au	11.58	1.18	73	10	1.22	1.87	0.65	[106]
ITO/TiO_2/$CsPbI_2Br$/Spiro/Au	12.7	1.05	68.4	9.08	1.05	1.92	0.87	[107]
ITO/TiO_2/$CsPbI_2Br$/PMMA/Spiro/Ag	15.8	1.07	74.5	12.6	1.07	1.82	0.75	[108]
FTO/NiO_x/$CsPbI_2Br$/ZnO@C_{60}/Ag	15.2	1.14	77	13.3	1.14	1.92	0.78	[68]
ITO/SnO_2/$CsPbI_2Br$/Spiro/Ag	15.99	1.06	77.12	13.09	1.17	1.91	0.74	[109]
ITO/TiO_2/$CsPbI_2Br$/Spiro/Ag	13.99	1.1	67.25	10.34	1.1	1.97	0.87	[110]
FTO/TiO_2/m-TiO_2/$CsPbI_2Br$/Spiro/Ag	11.89	1.11	75	9.84	1.11	1.92	0.81	[111]
FTO/TiO_2/$CsPbI_2Br$/P3HT/Au	11.5	1.005	67	7.7	1.005	1.87	0.905	[112]
ITO/Ca/C_{60}/$CsPbI_2Br$/TAPC/TAPC:MoO_3/Ag	15.2	1.13	68	11.8	1.13	1.91	0.78	[98]
FTO/NiMgLiO/$CsPbI_2Br$/PCBM/BCP/Ag	14.18	0.98	66	9.14	0.98	1.91	0.93	[32]
FTO/TiO_2/$CsPbI_2Br$/C	13.54	1.15	64.2	10	1.19	1.905	0.715	[38]
FTO/TiO_2/$CsPb_{0.98}Sr_{0.02}I_2Br$/P3HT/Au	14.9	1.067	70.9	11.3	1.067	1.88	0.813	[113]
FTO/TiO_2/$CsPbI_2Br$/$CsPbI_2Br$ QDs/PTAA/Au	14.37	1.172	80	13.47	1.172	1.91	0.738	[51]
FTO/TiO_2/m-TiO_2/$CsPbI_{1.78}BrF_{0.22}$/Spiro/Ag	14.94	1.01	68	10.26	1.02	1.84	0.82	[114]
FTO/TiO_2/$CsPbI_2Br$/Spiro/Ag	13.61	1.13	68.64	10.56	1.13	1.82	0.69	[115]
ITO/NiO_x/$CsPbI_2Br$/C_{60}/BCP/Ag	12.6	1.05	78.7	10.4	1.05	1.9	0.85	[116]
FTO/TiO_2/$CsPbI_2Br$/Spiro/Au	15.57	1.18	74.56	13.69	1.18	1.9	0.72	[117]
PET/ITO/Nb_2O_5/$CsPbI_2Br$/Spiro/Au	14.61	1.19	67.25	11.73	1.21	1.9	0.69	
ITO/SnO_2/$CsPbI_2Br$/PTAA/Au	15.565	1.162	79.06	14.3	1.162	1.91	0.748	[118]
ITO/PEDOT:PSS/$CsPbI_2Br$/PCBM/BCP/Al	10.9	1.06	58.8	6.8	1.06	1.9	0.84	[119]
ITO/SnO_2/$CsPbI_2Br$/Spiro/Au	15.22	1.22	76.58	14.21	1.22	1.91	0.69	[13]
FTO/TiO_2/$CsPbI_2Br$ QDs/Spiro/Au	5.32	1.3	77	5.34	1.31	1.85	0.54	[72]
FTO/TiO_2/$CsPbI_2Br$ QDs/Spiro/MoO_3/Ag	11.72	0.97	62	7.04	0.97	1.92	0.95	[100]
ITO/SnO_2/PN4N/$CsPbI_2Br$/PDCBT/MoO_3/Ag	15.3	1.3	81.5	16.2	1.3	1.92	0.62	[20]

Table 2. Continued.

Cell structure	J_{sc} [mA cm^{-2}]	V_{oc} [V]	FF [%]	PCE [%]	Highest V_{oc} [V]	Bandgap [eV]	E_{loss} [eV]	Ref.
FTO/NiMgLiO/$CsPbI_2Br$/C–MOX/Ag	14.72	1.26	76	14	1.26	1.9	0.64	[7]
FTO/TiO_2/m-TiO_2/BaI_2:$CsPbI_2Br$/P3HT/Au	15.45	1.21	79.45	14.85	1.21	1.92	0.71	[120]
FTO/TiO_2/$CuBr_2$ $CsPbI_2Br$/Spiro/MoO_3/Ag	16.95	1.18	80	16.15	1.18	1.95	0.77	[121]
ITO/SnO_2/$CsPbI_2Br$/CsBr/Spiro/Au	16.72	1.271	77.18	16.37	1.271	1.88	0.609	[122]

at the CsBr solution/PbI_2/$PbBr_2$ interface and helps the CsBr precursor diffuse further into the PbI_2/$PbBr_2$ layer, resulting a uniform nucleation rate of $CsPbI_xBr_{3-x}$ crystal. Based on high-quality perovskite films, the device presented a high efficiency of 13.27% with high V_{oc} of 1.32 V.[34] Furthermore, Yin et al. directly synthesized the PbI_2(DMSO) and $PbBr_2$(DMSO) adducts as precursors and effectively reduced the fast reaction rate between PbI_2, $PbBr_2$, and CsI. A high-quality $CsPbI_2Br$ perovskite film with large grain size and low defect density was obtained, thus leading to the high V_{oc} 1.22 V with a high PCE 14.78%.[35]

The solvent evaporation rate is closely associated with the nucleation and crystal growth of the perovskite. When only DMF with fast volatilization is used, CsX (X = Br, I) tends to react with PbX_2 quickly, forming lots of small $CsPbI_2Br$ crystal nucleus, thus resulting in the small crystal grain size in the final films. In order to optimize the procedures of deposition of $CsPbI_2Br$ films, Tian et al. systematically investigated the effects of the ratio of DMF/DMSO and the precursor concentration. They realized a wide solution processing window for excellent performance along with the super high V_{oc} of 1.315 V with PCE reaching 12.52% (**Figure 3**a,b).[33]

Besides the content of DMSO, the precursor solution temperature also influences the solvent evaporation. The correlation between crystallization and precursor solution temperature was clearly studied by Bai et al. As shown in Figure 3c, after a series of optimizations, they found improved crystallization of $CsPbI_2Br$ could be realized, when the precursor solution temperature was 100 °C. Finally, the V_{oc} was risen from 1.18 to 1.22 V with enhanced PCE 14.81% due to the reduced grain boundaries.[36]

Apart from focusing on the optimization of precursor solution, antisolvent methods are also used to prepare of high-quality perovskite film, which has been well established in the preparation of HPSC films.[37] In this method, nonpolar solvents are utilized to rapidly reduce the solubility of perovskite in solution and accelerate the nucleation and crystal growth of perovskite. The Zhao group applied this method to $CsPbI_2Br$ IPSCs, they found a green solvent, instead of the chlorobenzene, ethyl acetate could also promote the film quality. Compared to the films obtained without antisolvent and chlorobenzene treatment, the ethyl acetate treated $CsPbI_2Br$ films exhibited excellent crystallinity with large grains, dense and uniform surface. Consequently, the V_{oc} of 1.15 V was increased by 0.23 V versus without antisolvent treatment and 0.13 V versus chlorobenzene treatment, respectively.[38]

The essence of the solvent engineering strategy is to optimize the grain nucleation process and grain growth process

Table 3. Photovoltaic parameters and E_{loss} of $CsPbIBr_2$ IPSCs.

Cell structure	J_{sc} [mA cm^{-2}]	V_{oc} [V]	FF [%]	PCE [%]	Highest V_{oc} [V]	Bandgap[eV]	E_{loss} [eV]	Ref.
FTO/TiO2/$CsPb_{0.995}Mn_{0.005}I_{1.01}Br_{1.99}$/C	13.15	0.99	57	7.36	0.99	1.85	0.86	[123]
FTO/In_2S_3/$CsPbIBr_2$/Spiro/Ag	7.76	1.09	65.94	5.59	1.09	2.08	0.99	[124]
FTO/TiO_2/$CsPbIBr_2$/C	11.17	1.283	60	8.6	1.283	2.05	0.767	[39]
FTO/TiO_2/$CsPbIBr_2$/Spiro/Au	9.69	1.227	67.4	8.02	1.227	2.05	0.823	[125]
FTO/TiO_2/$CsPbIBr_2$/Au	8.7	0.959	56	4.7	0.959	2.05	1.091	[126]
FTO/TiO_2/m-TiO_2/$CsPbIBr_2$/Spiro/Au	7.9	1.121	70	6.3	1.121	2.05	0.929	[127]
FTO/NiO_x/$CsPbIBr_2$/MoO_x/Au	10.56	0.85	62	5.52	0.85	2.08	1.23	[128]
FTO/TiO_2/$CsPbIBr_2$/C	10.66	1.245	69	9.16	1.245	2.05	0.805	[129]
FTO/NiO_x/$CsPbIBr_2$/ZnO/Al/ITO	8.65	1.01	63.6	5.57	1.01	2.05	1.04	[130]
FTO/TiO_2/m-TiO_2/$CsPb_{0.9}Sn_{0.1}IBr_2$/C	14.3	1.26	63	11.33	1.27	1.79	0.52	[44]
FTO/TiO_2/m-TiO_2/$CsPbIBr_2$/C	12.32	1.08	62	8.25	1.08	1.9	0.82	
ITO/SnO_2/C_{60}/$CsPb_{0.75}Sn_{0.\ 25}IBr_2$/Spiro/Au	12.57	1.21	75.8	11.53	1.21	1.78	0.57	[45]
FTO/TiO_2/$SmBr_3$/$CsPbIBr_2$/PTAA	12.75	1.17	73	10.88	1.17	2.11	0.94	[16]
FTO/TiO_2/$CsPbIB_2$/Spiro/Au	8.8	1.28	64.9	7.31	1.28	2.07	0.79	[40]
FTO/TiO_2/$CsPbIBr_2$ QDs/Spiro/MoO_3/Ag	9.31	0.96	59	5.27	0.96	2.33	1.37	[100]
ITO/SnO_2/$CsPbIBr_2$/Spiro/Ag	10.69	1.267	71	9.86	1.267	2.07	0.803	[131]

Table 4. Photovoltaic parameters and E_{loss} of $CsPbI_xBr_{3-x}$ IPSCs.

Cell structure	J_{sc} [mA cm^{-2}]	V_{oc} [V]	FF [%]	PCE [%]	Highest V_{oc} [V]	Bandgap [eV]	E_{loss} [eV]	Ref
FTO/TiO_2/$CsPbI_{1.8}Br_{1.2}$/PTAA/Au	12.3	1.288	65	10.3	1.288	2.16	0.872	[132]
FTO/TiO_2/$CsPbI_{1.5}Br_{1.5}$/PTAA/Au	11	1.282	65	9.1	1.282	2.1	0.818	
FTO/TiO_2/$CsPbI_{1.2}Br_{1.8}$/PTAA/Au	9.7	1.332	64	8.2	1.332	2.02	0.688	
FTO/TiO_2/$CsPbI_{3-x}Br_x$/Spiro/Au	16.46	0.98	67.54	10.92	0.99	1.79	0.8	[133]
FTO/TiO_2/$CsPbI_{1.5}Br_{1.5}$ QDs/Spiro/MoO_3/Ag	11.35	1	70	7.94	1	2.19	1.688	[100]

Table 5. Photovoltaic parameters and E_{loss} of $CsPbBr_3$ IPSCs.

Cell structure	J_{sc} [mA cm^{-2}]	V_{oc} [V]	FF [%]	PCE [%]	Highest V_{oc} [V]	Bandgap [eV]	E_{loss} [eV]	Ref.
FTO/m-TiO_2/$CsPbBr_3$/PTAA/Au	6.24	1.28	74	5.95	1.28	2.36	1.08	[134]
FTO/TiO_2/m-TiO_2/$CsPbBr_3$/PTAA/Au	6.7	1.25	72	6.1	1.26	2.36	1.1	[135]
FTO/TiO_2/$CsPbBr_3$ QDs/Spiro/Au	5.653	1.536	62.4	5.42	1.536	2.38	0.844	[74]
FTO/TiO_2/m-TiO_2/GQDs/$CsPbBr_3$/C	8.12	1.458	82.1	9.72	1.458	2.3	0.842	[136]
FTO/TiO_2/m-TiO_2/$CsPbBr_3$/C	6.72	1.406	77.1	7.28	1.406	2.32	0.914	[137]
FTO/TiO_2/m-TiO_2/$Cs_{0.91}Rb_{0.09}PbBr_3$/C	7.73	1.552	82.2	9.86	1.552	2.24	0.688	
FTO/TiO_2/m-TiO_2/$Cs_{0.98}Li_{0.02}PbBr_3$/C	6.95	1.454	77.9	7.87	1.454	2.29	0.836	
FTO/TiO_2/m-TiO_2/$Cs_{0.94}Na_{0.06}PbBr_3$/C	6.97	1.49	80	8.31	1.49	2.27	0.78	
FTO/TiO_2/m-TiO_2/$Cs_{0.92}K_{0.08}PbBr_3$/cC	7.25	1.514	78.4	8.61	1.514	2.25	0.736	
FTO/ZnO NPs/$CsPbBr_3$-$CsPb_2Br_5$/Spiro/Au	6.17	1.43	77.2	6.81	1.43	2.3	0.87	[138]
FTO/TiO_2/$CsPbBr_3$/Spiro/Au	6.97	1.27	78.5	6.95	1.32	2.358	1.038	[139]
FTO/TiO_2/m-TiO_2/$CsPbBr_3$/C	5.7	1.29	68	5	1.29	2.3	1.01	[140]
FTO/TiO_2/$CsPbBr_3$/Spiro/Au	7.01	1.42	53	5.6	1.42	2.3	0.88	[141]
FTO/TiO_2/m-TiO_2/$CsPb_{0.97}Tb_{0.03}Br_3$/SnS:ZnS/NiO_x/C	8.21	1.57	79.6	10.26	1.57	2.3	0.73	[17]
FTO/TiO_2/m-TiO_2/$CsPbBr_3$/$CsSnBr_2I$ QDs/C	8.7	1.39	75.5	9.13	1.39	2.3	0.91	[65]
FTO/TiO_2/m-TiO_2/$CsPbBr_3$/MoS_2 QDs/C	6.55	1.307	79.4	6.8	1.307	2.3	0.993	[142]
FTO/TiO_2/m-TiO_2/CQDs/$CsPbBr_3$/RPQDs/C	7.33	1.47	76	8.2	1.47	2.3	0.83	[64]
FTO/TiO_2/m-TiO_2/$CsPbBr_3$/CdZnSe@ZnSe QDs/C	7.25	1.498	79.6	8.65	1.498	2.3	0.802	[66]
FTO/TiO_2/m-TiO_2/$CsPbBr_3$/C	7.4	1.24	73	6.7	1.24	2.3	1.06	[143]
FTO/TiO_2/m-TiO_2/Cl-$CsPbBr_3$/Spiro/Ag	8.47	1.02	71.6	6.21	1.02	2.32	1.3	[144]
FTO/TiO_2/GQDs/$CsPbBr_3$/CISZ-QDs/C	7.35	1.522	84.3	9.43	1.522	2.3	0.778	[145]
FTO/TiO_2/m-TiO_2/$CsPbBr_3$/PCBM/C	6.94	1.352	74.5	6.99	1.352	2.3	0.948	[25]
FTO/TiO_2/m-TiO_2/$CsPb_{0.97}Sm_{0.03}Br_3$/PCBM/C	7.48	1.594	85.1	10.14	1.594	2.3	0.706	
FTO/TiO_2/m-TiO_2/$CsPb_{0.97}Tb_{0.03}Br_3$/PCBM/C	7.47	1.588	84.8	10.06	1.588	2.3	0.712	
FTO/TiO_2/m-TiO_2/$CsPb_{0.97}Ho_{0.03}Br_3$/PCBM/C	7.45	1.572	83.2	9.75	1.572	2.3	0.728	
FTO/TiO_2/m-TiO_2/$CsPb_{0.97}Er_{0.03}Br_3$/PCBM/C	7.46	1.563	82.8	9.66	1.563	2.3	0.737	
FTO/TiO_2/m-TiO_2/$CsPb_{0.97}Yb_{0.03}Br_3$/PCBM/C	7.45	1.536	80.2	9.2	1.536	2.3	0.764	
ITO/PEDOT:PSS/$CsPbBr_3$/PCBM/Ag	5.9	0.982	73.7	4.5	0.982	2.3	1.318	[146]
FTO/TiO_2/$CsPbBr_3$-$CsPb_2Br_5$/Spiro/Ag	8.48	1.296	75.9	8.34	1.296	2.4	1.104	[147]
ITO/ZnO/$CsPbBr_3$/Spiro/Au	7.01	1.44	77.11	7.78	1.44	2.36	0.92	[148]
ITO/TiO_2/m-TiO_2/$CsPbBr_3$ QDs/Spiro/Au	8.55	0.859	0.57	4.21	0.859	2.4	1.541	[22c]
FTO/TiO_2/m-TiO_2/$CsPbBr_3$/C	7.34	1.25	63	5.82	1.25	2.34	1.09	[44]
ITO/SnO_2/$CsPbBr_3$/Spiro/Au	10.33	1.26	75.34	9.81	1.26	2.3	1.04	[13]
FTO/TiO_2/$CsPbBr_3$ QDs/Spiro/MoO_3/Ag	7.38	0.9	40	2.65	0.9	2.39	1.49	[100]

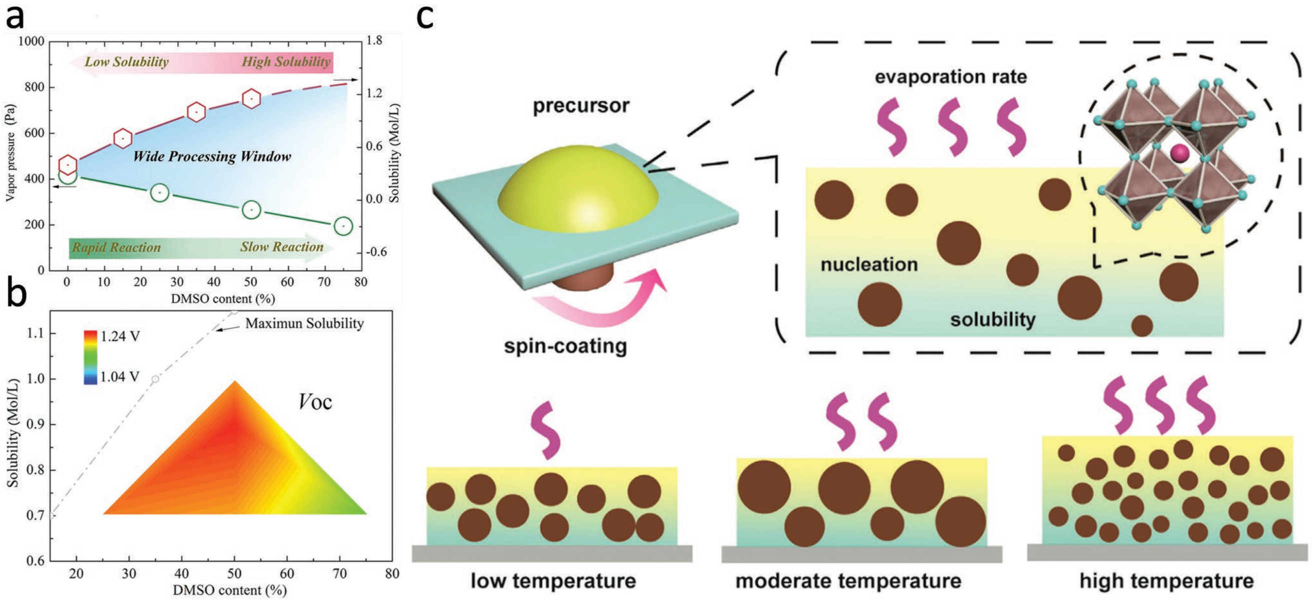

Figure 3. a) Vapor pressure for mixed solvent and solubility for $CsPbI_2Br$ as a function of DMSO content. b) V_{oc} of the wide solution-processing window dependence on the DMSO content and $CsPbI_2Br$ solubility. Reproduced with permission.[33] Copyright 2018, American Chemical Society. c) Growth mechanism of thin $CsPbI_2Br$ film with spin-coating processing: schematic illustration of correlation between external factors (solubility and solvent evaporation rate) and nucleation and film growth at different film temperatures. Reproduced with permission.[36] Copyright 2018, Elsevier Inc.

to improve the film crystallinity and morphology. Apart from the management on the states of precursor solution, annealing process of the as-prepared films also plays an important role on the final film quality. Therefore, a precise control of annealing process is necessary for high-quality film.

3.1.2. Annealing Engineering

During the fabrication of perovskite films, the annealing process makes the precursor crystallize into perovskite-phase grains and promotes the growth of grains. So annealing process is critical to the quality of perovskite film. Due to the high boiling point of DMSO (DMF 153 °C, DMSO 189 °C), it cannot escape from the precursor film immediately at room temperature after spin-coating. The residual DMSO can help the mass transport and diffuse during the annealing process. In this case, high-quality film can be achieved through the precursor control on the evaporation rate. You et al. developed a solvent-controlled growth (SCG) method through placing inorganic perovskite precursor films in the nitrogen glove box for several ten minutes before annealing (**Figure 4**a). Comparing the films without SCG, the films with SCG showed better quality with a large crystal size above 5 µm and no pinholes(Figure 4b–e). The V_{oc} increased from 0.91 V to 1.08 V and, correspondingly, the PCE increased from 8.58% to 15.7%.[13] Based on the similar idea, the Hao group proposed a light-processing strategy to promote the mass transport and film quality (Figure 4f), and achieved a V_{oc} of 1.283 V, which is the highest V_{oc} in $CsPbIBr_2$ IPSCs.[39]

Although, several groups find the content of residual DMSO plays an important role in film quality, the excess DMSO in precursor film will severely restrain precursor dispersion, resulting in nucleation aggregation and solvent edge effects across the entire film, even if the gradient thermal annealing method (GTA) is applied. To solve this problem, Chen et al. also reported an antisolvent treatment strategy (ATS) to wash away the excess residual DMSO by low-boiling-point solvent (such as toluene and isopropanol). After IPA treatment, only trace DMSO remained in $CsPbI_2Br$-precursor film. The initial ATS-IPA process could homogeneously “freeze” the perovskite precursor onto the substrate and eliminate the solvent edge effect to improve the morphology of the $CsPbI_2Br$ film. The subsequent GTA process could control the growth of the crystal by slowing down the DMSO evaporation rate. Finally, through this GTA-ATS-IPA synergetic procedure, a $CsPbI_2Br$ film with large crystalline grains and low defect density was achieved, thus obtaining a V_{oc} of 1.23 V and a high PCE of 16.07% for $CsPbI_2Br$ IPSCs.[14]

3.1.3. Additives/Doping Engineering

Besides solvent and annealing engineering, the introduction of additives or metal ions into precursor solution is another effective strategy to improve perovskite film quality. The Zheng group added polymer polyethylene glycol (PEG) into $CsPbIBr_2$ precursor solution. The PEG not only serves as a matrix to slow down crystal growth, but also promotes the film-forming property of $CsPbIBr_2$ solution, thus leading to a high-quality $CsPbIBr_2$ film. The improved device presented a V_{oc} of 1.28 V with no sacrifice of J_{sc} and *FF*, while V_{oc} was only 1.10 V for controlled device. Correspondingly, the PCE was increased to 7.31% from 6.36%.[40] In addition, the introduction of ethylenediamine cations (EDA^{2+}) into $CsPbI_3$ films can not only stabilize cubic perovskite phase of $CsPbI_3$, but improve film

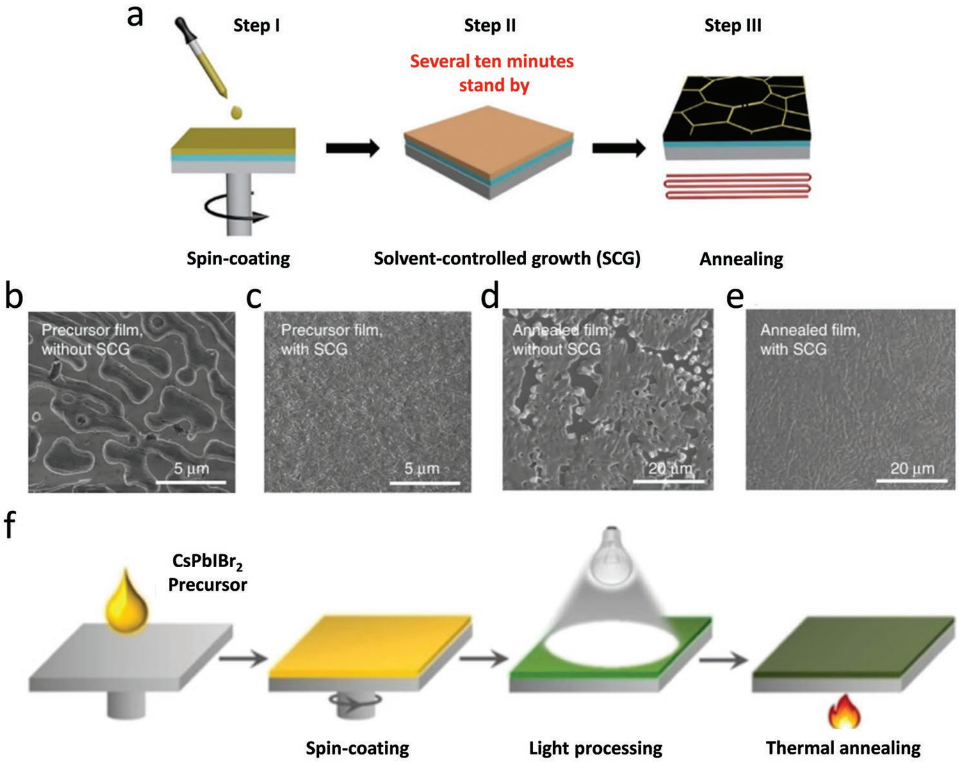

Figure 4. a) A schematic illustration of $CsPbI_3$ crystallization procedures via solvent-controlled growth (SCG). b,c) SEM images of $CsPbI_3$ precursor film without and with SCG. d,e) SEM images of annealed $CsPbI_3$ precursor films without and with SCG. Reproduced with permission.[13] Copyright 2018, Springer Nature. f) Schematic formation procedures of $CsPbIBr_2$ film by light-processing strategy. Reproduced with permission.[39] Copyright 2019, American Chemical Society.

morphology, thus achieving a V_{oc} of 1.15 V with E_{loss} of 0.58 eV and a high PCE of 11.86%.[41] Organic additives strategy can boost the film quality and the humidity stability at the same time, and show a great potential for further improvement on device performance.

Apart from the organic molecules and polymers, the ion doping is also an useful means to improve film quality. Tang group systematically studied the effect of alkali metal cations (Li^+, Na^+, K^+, and Rb^+) doping on the performance of $CsPbBr_3$ IPSCs. All these doping ions could improve photoelectronic property of $CsPbBr_3$ through making the lattice volume contracted and increase the formation energy of crystal nucleation. Therefore, $Cs_xA_{1-x}PbBr_3$ (A = Li^+, Na^+, K^+, Rb^+) perovskite crystal tended to grow into larger grain driven by the existed crystal surface. As the lattice constants decreased, the corresponding grain became larger and thus the value of V_{oc} increased from 1.406 V for $CsPbBr_3$ to 1.552 V for $Cs_{0.91}Li_{0.09}PbBr_3$.[39] In addition, Khan et al. found that $MnCl_2$-$ZnCl_2$ doping could also reduce trap density and suppress the recombination by modulating the $CsPbI_2Br$ crystal growth, obtaining a V_{oc} of 1.23 V and high PCE of 14.15%.[42] The similar function could be realized through lanthanide ions doping in $CsPbBr_3$, reported by Duan et al. They systematically studied the performance of lanthanoid doped $CsPbBr_3$ IPSCs, a V_{oc} of 1.594 V (Pristine 1.352 V) with PCE of 10.14% was achieved by Sm^{3+} doping.[25]

In addition, lots of IPSCs exhibit improved PCE through the ion doping. For example, Tang group achieved a high V_{oc} of 1.57 V for $CsPb_{0.97}Tb_{0.03}Br_3$ solar cells. They ascribe the high V_{oc} to the unique intermediate energy levels introduced by Tb^{3+}, which can serve as a temporary carrier reservoir allowing for long carrier lifetimes.[17] Doping/alloying Bi^{3+} or Sn^{2+} ions can obviously narrow the bandgaps and decrease the E_{loss}, such as $CsPb_{0.96}Bi_{0.04}I_3$ IPSCs (E_g =1.56 eV, E_{loss} = 0.56 eV[11] and 0.51 eV[43]), $CsPb_{0.9}Sn_{0.1}IBr_2$ IPSCs (E_g = 1.79 eV, E_{loss} = 0.52 eV),[44] and $CsPb_{0.75}Sn_{0.\ 25}IBr_2$ IPSCs (E_g = 1.78 eV, E_{loss} = 0.57 eV).[45] Nevertheless, a little part of doped perovskite devices present decreased V_{oc}. Duan group found that the general alkaline earth ions doping can also enlarge grain size to the same level as lanthanoid doping, but the carrier lifetime is lower, which means more defects are introduced.[25] The doping engineering shows great potential in boosting the V_{oc}, but the deep mechanism is still not clear. Maybe the improved electronic structure of the doped perovskite is vital. Because the valence band of $CsPbX_3$ (X = Cl, Br, I) is mainly composed of X *n*p (*n* = 3,4,5) and Pb 6s orbital, and the conduction band is determined by antibonding mixing of Pb 6p and X *n*p orbital, with a major contribution from Pb 6p orbital.[46] The substitute of Pb^{2+} by doped ions can affect integral energy states, which influence the electronic structure or bulk defect states inside the grain.[47] It is significant to find out the truth behind the high V_{oc} by doping, which may inspirit us new ways to further minimize the E_{loss}.

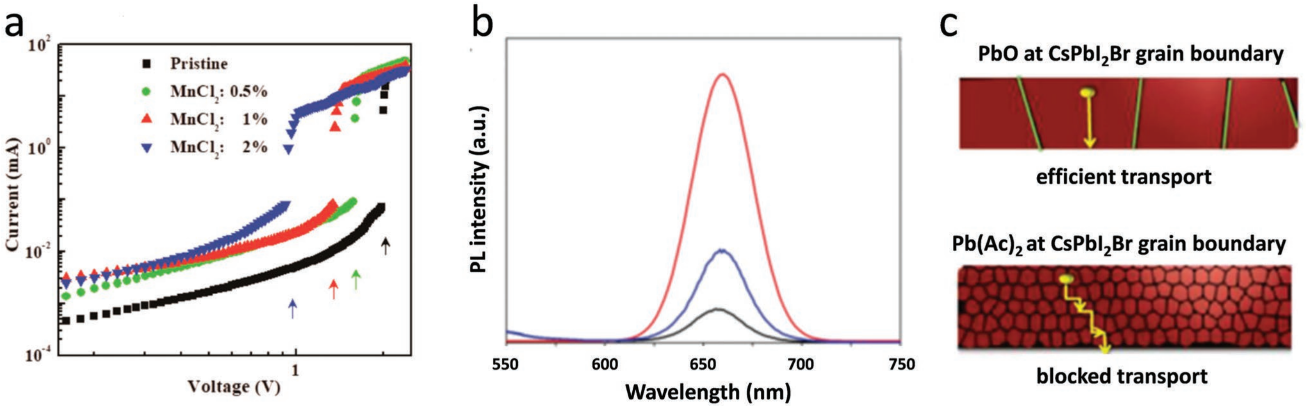

Figure 5. a) Dark *I–V* measurements of the devices with V_{TFL} kink point behavior. Reproduced with permission.[51] Copyright 2018, American Chemical Society. b) PL spectra of the films on glass. c) A schema of charge transport property in PbO-and Pb(Ac)$_2$-modified films. Reproduced with permission.[53] Copyright 2018, Wiley-VCH.

3.2. Defect Passivation

Even though lead halide perovskites are widely regarded as "defect-tolerant" materials, defects can also formed at the grain boundary, as above mentioned in the part of Section 3.1.[29] So far, three point defects (vacancies, interstitials and antisites) are known as trap states in inorganic perovskites in theory. Among them, the vacancies have low formation energy and therefore are widely existed. Due to the perovskite special electronic structure, the vacancies are always shallow defects within the bandgap, implying the trapped charges can still be relaxed easily to valence band or conduction band and contribute to J_{sc}. But the band tails caused by these shallow defects is harmful to carrier mobility and the V_{oc}. The interstitial and antisite defects are known as the deep defects and account for the capture of carriers and Shockley-Read-Hall recombination.[28,46,48] But these two defects have high formation energies and are hard to be formed. All the defects can result in E_{loss}. So, in this part, we summarize the efficient methods for defects passivation in IPSCs.

3.2.1. Grain Boundary Passivation

The lead halide perovskites are ionic structure crystals, therefore, many groups adopt metal ions doping method to passivate the grain boundary. Hayase group achieved a V_{oc} of 1.34 V in CsPbBrI$_2$ solar cells by doping or alloying Ge^{2+}, which is the highest value for CsPbBrI$_2$ IPSCs. Though the introduce of Ge^{2+} reduce the grain size, suppressed nonradiative recombination is realized. Similar results are observed by Hagfeldt group through doping Eu^{2+}.[49,50] In addition, Bai et al. demonstrated that adding Mn^{2+} into the precursor solution can significantly improve the V_{oc} from 1.115 to 1.172 V as well as the PCE from 11.88% to 13.47%. The Mn^{2+} can insert into the interstices of the CsPbI$_2$Br lattice and suppress the nucleation process, leading to improved crystallinity. The existence of Mn^{2+} has no adverse effect on the conductivity of the perovskite film, because the electronic states introduced by Mn^{2+} is located below the valence band maximum, showing negligible contribution to band edges. Apart from the doped Mn^{2+}, the excessive Mn^{2+} aggregates at the grain boundaries and surface of the CsPbI$_2$Br film and passivate the electron trap states, as the lower trap-filled limit voltage (V_{TFL}) presented in **Figure 5**a.[51]

In addition to metal ions, the polymer poly-vinylpyrrolidone (PVP) is proved to passivate the grain boundary of CsPbI$_3$ by interacting with Cs$^+$ ions[52] Han group found the additives Pb(Ac)$_2$ can strongly coordinate with CsPbI$_2$Br through Cs-Ac bond, compared with controlled device, the V_{oc} increased from 0.97 to 1.01 V. However, the Pb(Ac)$_2$ with Ac$^-$ organic group is an insulator modified at grain boundaries, where the carrier transport is hindered. After increasing the annealing temperature to 350 °C, the PbO (semiconductor with bandgap 2.6 eV) will in situ form at the grain boundaries by decomposing the Pb(Ac)$_2$. Although the PbO passivation effect is poorer than Pb(Ac)$_2$, the charge transport ability is enhanced due to the enlarged grains with less grain boundaries (Figure 5b,c). As a result, the V_{oc} further increases by 0.16 V, thus resulting a PCE enhancement from 8.7% to 12.0%.[53]

3.2.2. Surface Defect Passivation

Compared with the defects passivation on the grain boundaries, elimination of surface trap states is of equal importance to promote charge collection and reduce E_{loss}. Two strategies are designed for surface defect passivation. One is surface treatment with organic molecular or salts, and the other is the natural passivation effect of carrier transport layer.

Zhao group reported a facile approach to passivate the CsPbI$_3$ films with enhanced performance (PCE from 11.2% to 14.3%, V_{oc} from 1.02 to 1.11 V) through phenylethylammonium iodide (PEAI) treatment. They proposed that the phenylethylamine cation (PEA$^+$) and I$^-$ can passivate the Cs$^+$ and I$^-$ vacancies, respectively. The organic cation terminated surface resulted longer carrier lifetime without detriment of carrier transport and collection efficiency (**Figure 6**a,b).[54] Furthermore, they also found the PTABr can passivate the CsPbI$_3$ surface defects more efficiently and achieved the highest PCE of 17.06% in IPSCs with V_{oc} = 1.104 V.[12] Besides organic molecular, the Pb^{2+} can passivate the surface defect through Pb(NO$_3$)$_2$ methyl acetate solution treatment as reported by the trap density of CsPbI$_2$Br

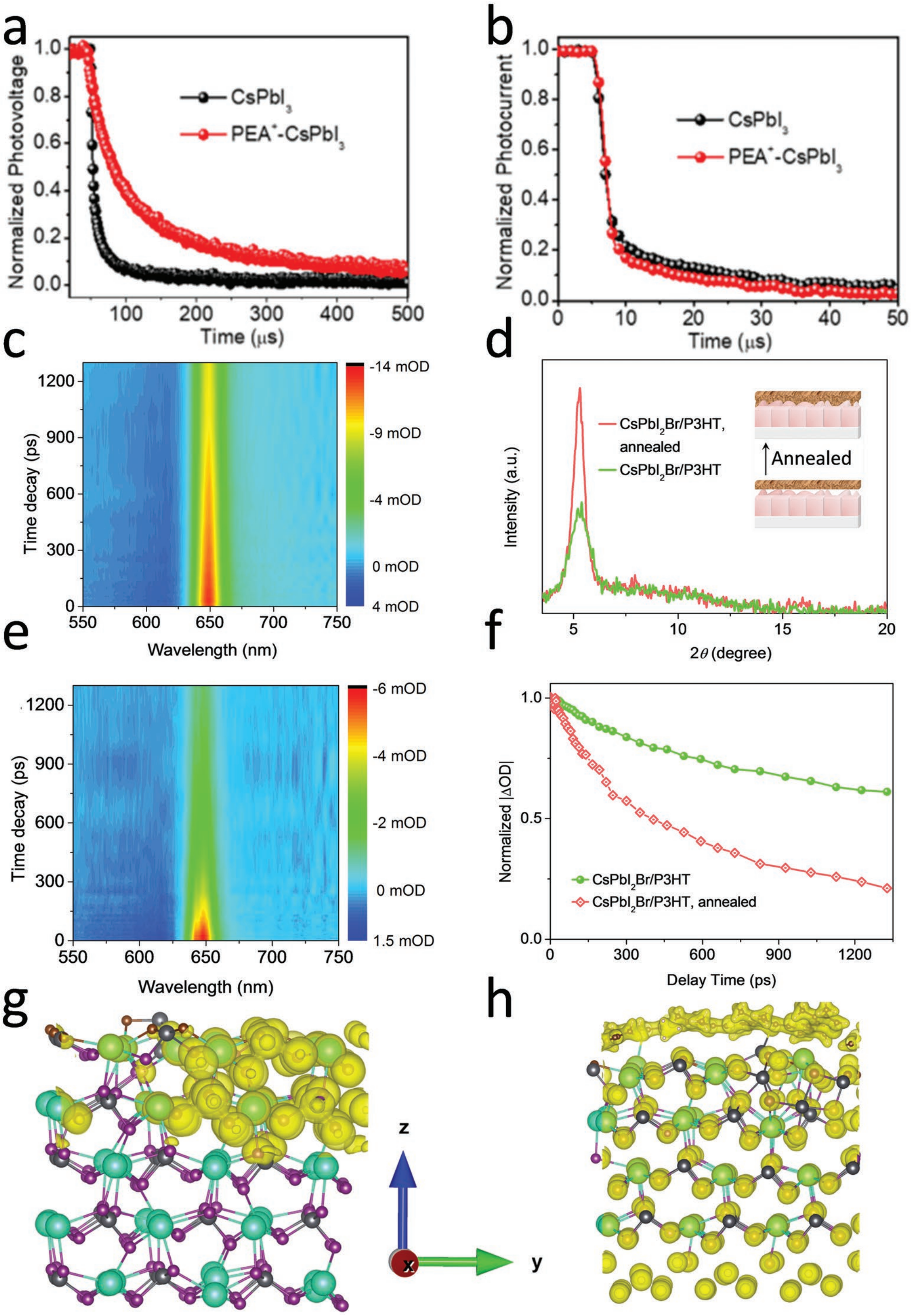

Figure 6. a) TPV of $CsPbI_3$- and PEA^+-$CsPbI_3$-based PSC devices. b) TPC of $CsPbI_3$- and PEA^+-$CsPbI_3$-based PSC devices. Reproduced with permission.[54] Copyright 2018, Elsevier Inc. c) Spectro-temporal transient absorption maps for $CsPbI_2Br$/P3HT bilayers before annealing. d) XRD patterns of P3HT films before and after annealing on $CsPbI_2Br$ substrates. e) Spectro-temporal transient absorption maps for $CsPbI_2Br$/P3HT bilayers after annealing. f) Characteristic dynamics for $CsPbI_2Br$/P3HT bilayers. g) No P3HT on 110-surface with antisite defects. h) P3HT on 110-surface with antisite defects. Reproduced with permission.[56] Copyright 2018, Wiley-VCH.

perovskite decreasing from 8×10^{16} to 6.64×10^{16} cm^{-3} and the E_{loss} is reduced from 0.68 to 0.62 eV.[55]

The lowest E_{loss} of $CsPbI_2Br$ is achieved by Zeng et al. through direct passivation effect of the hole transport layer poly(3-hexylthiophene) (P3HT). They studied the spectral distribution of photoexcited carriers in $CsPbI_2Br$/P3HT films using femtosecond broadband transient absorption (TA) spectroscopy. The TA 2D color maps show no redshift for the transient bleach peak (Figure 6c), indicating a flat energy landscape and negligible tail states below the bandgap. A further P3HT annealing process mitigates the energy disorder through improving the crystallinity and reducing structural disorder of P3HT (Figure 6d), thus leading to a more efficient hole transfer. The decay dynamics of the TA are much faster for the annealed bilayer (Figure 6e,f). To further investigate the passivation effect, they study the electronic structure based on density function theory (DFT) to characterize how P3HT passivate the $CsPbI_2Br$ surface. The S atom of P3HT can not only bond with Cs^+ to passivate positively charged under-coordinated Cs^+ ions but also bond with Pb^{2+} to eliminate antisite defects, the most detrimental defects. As shown in Figure 6g,h, electron distribution is localized around the Pb-Br antisite defects. Once P3HT is introduced, the electron distribution becomes delocalized, indicating the defects are passivated. Finally, a highest V_{oc} 1.32 V with lowest E_{loss} of 0.5 eV in $CsPbI_2Br$ IPSCs is obtained.[56] Above works focus on the surface modification between active layer and hole transport layer, the surface passivation near electron transport layer should also be conducted to improve the charge transfer and device performance. Furthermore, Yip group proposed a dual interfacial passivation method through introducing amino-functionalized polymer (PN4N) as cathode interlayer and poly[5,5′-bis(2-butyloctyl)-(2,2′-bithiophene)-4,4′-dicarboxylate-*alt*-5,5′-2,2′-bithiophene] (PDCBT) as hole transport layer. Both of the heteroatoms (N and S) in PN4N and PDCBT can interact with the $CsPbBrI_2$ perovskite and passivate the defects. Finally, the dual interfacial passivation strategy efficiently reduce the E_{loss} and enhance V_{oc} from 1.08 V to 1.30 V, and thus the PCE increases from 12.3% to 16.2%, which is the highest PCE of $CsPbI_2Br$ IPSCs. This work further highlights the importance of surface defect passivation on E_{loss} reduction. More attentions should be paid to explore the transport layer with proper functional group or atoms, such as "N", "S," or "Cl", which can interact with the perovskite layer and passivate the defects.

3.3. Interface Engineering

The strategies we have discussed above are all about reduction of defect density to decrease the E_{loss}. In addition, optimizing the energy level alignment between perovskite layer and charge transport layer is also of great importance to reduce the E_{loss}. The mismatched energy levels cause low charge extraction efficiency.[23,57] Under this circumstance, a large amount of charges will accumulate at the interface, thus leading to nonradiative recombination assisted by defects or, even worse, more direct electron-hole recombination. This will inhibit the quasi-Fermi level splitting and limit the V_{oc} and PCE.[58] Constructing interfacial layers with suitable energy-level with perovskites can not only effectively facilitate carrier injection but also offer an energy barrier that blocks charge carriers from flowing back, contributing to the reduction of recombination loss.[59,60]

Liu group first designed a $CsPbI_2Br$ bulk-nanosheet (NS)-quantum dot (QD) (3D–2D–0D) multiple graded interface to promote device performance (**Figure 7**a,b). They found that, compared to the 3D, 3D–2D, and 3D–0D structure, the 3D–2D–0D structure certainly exhibits a higher build-in potential calculated from Mott–Schottky capacitance measurement (Figure 7c), and more effective carrier extraction ability (Figure 7d), which is in accordance with the enhanced V_{oc} from 1.11 V to 1.19 V.[61] A larger build-in potential means an enhanced driving force for the separation of photogenerated carriers and an extended deletion region for reduced recombination, thus leading to enhanced charge extraction.[62] Furthermore, Liu group integrated $CsPbI_2Br$/$CsPbI_2Br$ QDs film together to realize an optimized energy alignment. Through the FAI surface treatment, the valence band of the surface active layer is further shifted upward and the surface defects are effectively passivated. As a consequence, decreased recombination loss and improved hole extraction efficiency are realized, thus achieve a high PCE of 14.12% with a high V_{oc} of 1.223 V.[63] In a similar way, Liao et al. introduced carbon quantum dots (CQDs) and redphosphorus quantum dots (RPQs) to the $CsPbBr_3$/TiO_2 and $CsPbBr_3$/Carbon interfaces, respectively, which accelerates both electron and hole transfer into interface layer. As a result, the V_{oc} is increased by ≈0.2 V.[64] There are many similar strategies using the quantum dots to optimize the energy level alignment and thus reduce the E_{loss}, such as $CsPbBr_3$/$CsSnBr_2I$ QDs bilayer,[65] $CsPbBr_3$/CdZnSe@ZnSe QDs bilayer,[66] $CsPbI_2Br$/$CsPbI_3$ QDs bilayer,[67] and so on.

A bi-transport layer with gradient energy level alignment is preferably adopted to enhance extraction of photogenerated electron and suppress interfacial trap-assisted recombination.[58,68] For example, Cao group introduced SnO_2/ZnO bilayer into the $CsPbI_2Br$ IPSCs architecture (Figure 7e), realizing a PCE over 14%. Compared with the SnO_2 monolayer IPSCs, the bilayer devices exhibit reduced trap-assisted recombination (smaller slope in V_{oc}–Light intensity curve) and more efficient charge extraction (larger slope in J_{sc}–Light intensity curve), which account for the V_{oc} increment from 1.06 to 1.23 V (Figure 7f).[58] Subhani et al. discovered a simple $SmBr_3$ modification method at TiO_2/$CsPbIBr_2$ interface can optimize the charge transfer process and suppress the nonradiative recombination. The $SmBr_3$ can diffuse into the perovskite layer with gradient concentration distribution, and result a gradient energy band alignment with hole blocking effect. Besides, the $SmBr_3$ can strengthen the connection between TiO_2 and perovskite, and thus enhance electron injection. The synergistic effect of optimized charge transfer process and suppressed nonradiative recombination enhances the V_{oc} by 0.12 V. The achieved PCE of 10.88% is the highest value in $CsPbIBr_2$ IPSCs.[16]

All the facts discussed above show that the heterojunction strategy is an effective way to minimize the E_{loss}. When there is a QD-modified layer, it can not only optimize the band alignment for V_{oc} increment but also absorb more sun light in other wavelength for J_{sc} increment. So the modifying device with QDs layer shows special advantage.

4. Conclusion and Outlook

In summary, the IPSCs have developed rapidly in recent years, especially for $CsPbI_3$ and $CsPbI_2Br$ cells, but the large E_{loss} hinder their further efficiency improvement. We have systematically reviewed the available strategies of managing E_{loss} in IPSCs, including the improvement of film quality, defect

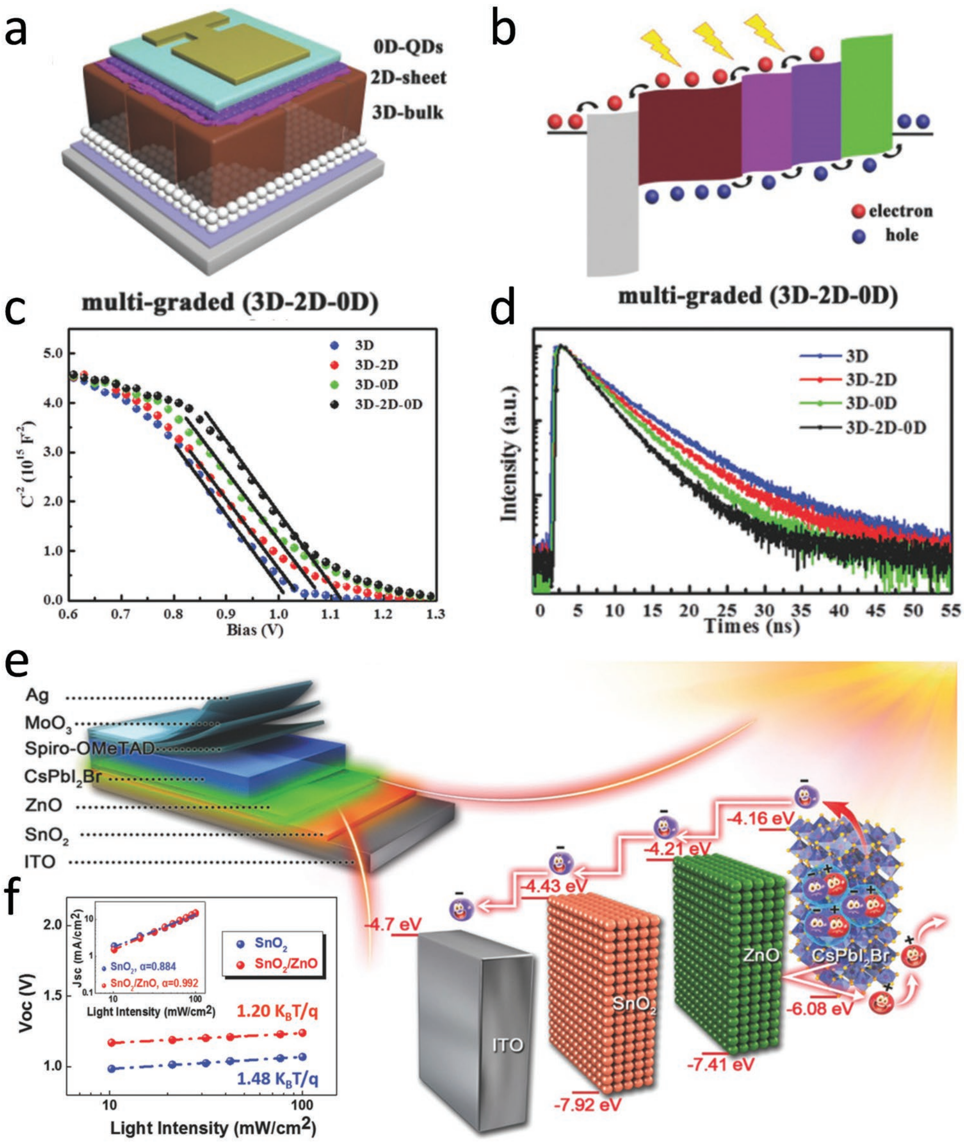

Figure 7. a) Schematic structures of devices without and with a graded interface. b) Schematic of the carrier transport mechanism in multigraded $CsPbBrI_2$ PSCs. c) Mott–Schottky fitting to the *C–V* data. d) TRPL curves of $CsPbBrI_2$ films. Reproduced with permission.[61] Copyright 2018, Wiley-VCH. e) Device architecture of the all-inorganic $CsPbI_2Br$ PVSC and the corresponding energy diagrams. f) Light intensity–dependent *J–V* properties of SnO_2- and SnO_2/ZnO-based $CsPbI_2Br$ PVSCs. Reproduced with permission.[58] Copyright 2018, Wiley-VCH.

passivation and interface engineering. In spite of rapid progress, there is still a long way to reduce E_{loss} and promote efficiency. More works should focus on improvement of inorganic perovskites in the future. The deep reasons for the large E_{loss} need to be further explored in both experiment and theory.

1. The physical properties of inorganic perovskites need to be understood deeply through more advanced and detailed theoretical calculations or experiments. Because of smaller ion radius of Cs^+ than that of MA^+ and FA^+, the Pb-X octahedrons tend to twist and collapse at room temperature. This makes crystal structure of $CsPbX_3$ deviate from cubic phase, and excess disorder are introduced. Is this the essential and key factor limiting the device performance or not, further works need to be done.
2. In particularly, when compared to the HPSCs, the E_{loss} problem is even more prominent. On the one hand, due to the larger bandgap of inorganic $CsPbX_3$ than that of MA- and FA-based hybrid perovskites, less electron–hole pairs will be generated in $CsPbX_3$. This results in a lower photogenerated carrier density in the bands, which enlarge the energy difference between E_{Fn}/E_{Fp} and the band edges, thus leading to reduced V_{oc} in inorganic perovskites.[19] Apart from the bandgap factor, the essential material properties account for the E_{loss} in solar devices. Grumstrup and coworkers have investigated the transport and relaxation dynamics in inorganic $CsPbI_2Br$ microcrystals by pump-probe microscopy.[69] In contrast to $MAPbI_3$, whose dominant relaxation pathway is a second-order, direct process,[70] the domination recombination mechanism of $CsPbI_2Br$ is via defect-assisted

nonradiative (Shockley-Read-Hall) recombination.[69] And the ambipolar mobility (5–15 cm^2 V^{-1} s^{-1}) is about fivefold lower than that of $MAPbI_3$ (28–68 cm^2 V^{-1} s^{-1}).[71] The higher mobility of $MAPbI_3$ is attributed to its high static dielectric and short intrinsic carrier scattering time, which greatly reduce the influence of defects. In contrast, the static dielectric Cs-based inorganic perovskites is smaller, so the carrier transport and recombination is sensitive to the defects, which cause much stronger E_{loss} in inorganic perovskites.[69] So it is highly necessary to minimize the E_{loss} of IPSCs by reducing or passivating the defects.

3. Noting that the very high V_{oc} with low E_{loss} is always achieved in IPSCs devices, whose films are deposited from colloidal QDs.[10,26,72–75] Luther group first stabilized the $CsPbI_3$ in black-phase through QD strategy and fabricated $CsPbI_3$ QD IPSCs through a layer-by-layer method with PCE of 10.77% in 2016.[10] They further improved the photovoltaic performance of $CsPbI_3$ QDs through FAI treatment, and achieved the highest PCE of 13.4% with high V_{oc} of 1.22 V for $CsPbI_3$ QD device. The synthesis of $CsPbX_3$ QDs always requires a high Pb/Cs molar ratio of 4.34 to stabilize the QDs, and thus the QD surface is PbX_2-rich.[56] The excess PbX_2 can be maintained in the final perovskite films, which may account for the high V_{oc} of perovskite QDs based devices. It has been proved that appropriately excess PbI_2 added in HPSCs can suppress the trap states at grain boundaries.[59,76] But this method has not been widely adopted in IPSCs, so precise control on the composition may be the efficient way to further reduce E_{loss} and improve device performance.
4. In some cases, ions doping is an effective method in boosting the V_{oc} and minimizing the E_{loss}, especially for the Br-contained IPSC. Maybe the doped ion can optimize the electronic structure of the perovskite. But the deep mechanism is still not clear. It is of great important to find out how the doped ions affect the material properties and what is the determining factor for the effective ions doping on minimizing the E_{loss}. There should be a systematical studying both in theory and experiment to exploit the untapped potential of ions doping engineering. This is significant for us to draw a general conclusion: what kind of ions doping can further minimize the E_{loss}.
5. More works on the optimization of the interface between perovskite layer and carrier transport layer should be conducted. The perovskite film quality has already been promoted to a high level by solvent engineering, annealing engineering and additives engineering. So the passivation of surface defects and the better matched energy level are potential to further minimize the E_{loss}. In addition to the perovskite layer, the energy disorder in transport layer also contributes to the E_{loss} of IPSCs, and should be further minimized through efficient method or treatment in future works.

Acknowledgements

C.L. and Q.Z. contributed equally to this work. This work was financially supported by the National Science Foundation of China (NSFC) under Grant No. 51433003, the National Key Research and Development Program of China (2016YFB0401701), the Fundamental Research Funds for the Central Universities, JLU and JLUSTIRT (2017TD-06), and the Opening funds of State Key Laboratory of Applied Optics, Changchun Institute of Optics, Fine Mechanics and Physics, Chinese Academy of Science. This article is part of the *Advanced Materials Interfaces* Hall of Fame article series, which highlights the work of top interface and surface scientists.

Conflict of Interest

The authors declare no conflict of interest.

Keywords

defect passivation, energy loss, inorganic perovskites, interface engineering, review, solar cells

Received: June 30, 2019
Revised: August 7, 2019
Published online:

---

[1] A. Kojima, K. Teshima, Y. Shiral, T. Miyasaka, *J. Am. Chem. Soc.* **2009**, *131*, 6050.
[2] C. C. Stoumpos, C. D. Malliakas, M. G. Kanatzidis, *Inorg. Chem.* **2013**, *52*, 9019.
[3] a) Z. Chen, Q. Dong, Y. Liu, C. Bao, Y. Fang, Y. Lin, S. Tang, Q. Wang, X. Xiao, Y. Bai, Y. Deng, J. Huang, *Nat. Commun.* **2017**, *8*, 1890; b) L. Gu, Z. Fan, *Light: Sci. Appl.* **2017**, *6*, e17090.
[4] Q. Dong, Y. Fang, Y. Shao, P. Mulligan, J. Qiu, L. Cao, J. Huang, *Science* **2015**, *347*, 967.
[5] a) D. Yang, X. Li, W. Zhou, S. Zhang, C. Meng, Y. Wu, Y. Wang, H. Zeng, *Adv. Mater.* **2019**, *31*, 1900767; b) H. Sun, Z. Yang, M. Wei, W. Sun, X. Li, S. Ye, Y. Zhao, H. Tan, E. L. Kynaston, T. B. Schon, H. Yan, Z. H. Lu, G. A. Ozin, E. H. Sargent, D. S. Seferos, *Adv. Mater.* **2017**, *29*, 1701153.
[6] a) H. H. Fang, F. Wang, S. Adjokatse, N. Zhao, J. Even, M. A. Loi, *Light: Sci. Appl.* **2016**, *5*, e16056; b) C. Xie, P. You, Z. Liu, L. Li, F. Yan, *Light: Sci. Appl.* **2017**, *6*, e17023.
[7] S. Zhang, W. Chen, S. Wu, R. Chen, Y. Huang, Z. Yang, J. Li, L. Han, W. Chen, *J. Mater. Chem. A* **2019**, *7*, 18603.
[8] A. F. Akbulatov, S. Y. Luchkin, L. A. Frolova, N. N. Dremova, K. L. Gerasimov, I. S. Zhidkov, D. V. Anokhin, E. Z. Kurmaev, K. J. Stevenson, P. A. Troshin, *J. Phys. Chem. Lett.* **2017**, *8*, 1211.
[9] A. Marronnier, G. Roma, S. Boyer-Richard, L. Pedesseau, J. M. Jancu, Y. Bonnassieux, C. Katan, C. C. Stoumpos, M. G. Kanatzidis, J. Even, *ACS Nano* **2018**, *12*, 3477.
[10] A. Swarnkar, A. R. Marshall, E. M. Sanehira, B. D. Chernomordik, D. T. Moore, J. A. Christians, T. Chakrabarti, J. M. Luther, *Science* **2016**, *354*, 92.
[11] Y. Hu, F. Bai, X. Liu, Q. Ji, X. Miao, T. Qiu, S. Zhang, *ACS Energy Lett.* **2017**, *2*, 2219.
[12] Y. Wang, T. Zhang, M. Kan, Y. Zhao, *J. Am. Chem. Soc.* **2018**, *140*, 12345.
[13] P. Wang, X. Zhang, Y. Zhou, Q. Jiang, Q. Ye, Z. Chu, X. Li, X. Yang, Z. Yin, J. You, *Nat. Commun.* **2018**, *9*, 2225.
[14] W. Chen, H. Chen, G. Xu, R. Xue, S. Wang, Y. Li, Y. Li, *Joule* **2019**, *3*, 191.
[15] a) Y. C. Zhao, W. K. Zhou, X. Zhou, K. H. Liu, D. P. Yu, Q. Zhao, *Light: Sci. Appl.* **2017**, *6*, e16243; b) W. Zhou, Y. Zhao, X. Zhou, R. Fu, Q. Li, Y. Zhao, K. Liu, D. Yu, Q. Zhao, *J. Phys. Chem. Lett.* **2017**, *8*, 4122.
[16] W. S. Subhani, K. Wang, M. Du, X. Wang, S. Liu, *Adv. Energy Mater.* **2019**, *9*, 1803785.

[17] H. Yuan, Y. Zhao, J. Duan, Y. Wang, X. Yang, Q. Tang, *J. Mater. Chem. A* **2018**, *6*, 24324.
[18] G. E. Eperon, G. M. Paternò, R. J. Sutton, A. Zampetti, A. A. Haghighirad, F. Cacialli, H. J. Snaith, *J. Mater. Chem. A* **2015**, *3*, 19688.
[19] S. Rühle, *Sol. Energy* **2016**, *130*, 139.
[20] J. Tian, Q. Xue, X. Tang, Y. Chen, N. Li, Z. Hu, T. Shi, X. Wang, F. Huang, C. J. Brabec, H. L. Yip, Y. Cao, *Adv. Mater.* **2019**, *31*, 1901152.
[21] a) J. H. Heo, S. H. Im, J. H. Noh, T. N. Mandal, C.-S. Lim, J. A. Chang, Y. H. Lee, H.-j. Kim, A. Sarkar, M. K. Nazeeruddin, M. Grätzel, S. I. Seok, *Nat. Photonics* **2013**, *7*, 486; b) A. Marchioro, J. Teuscher, D. Friedrich, M. Kunst, R. van de Krol, T. Moehl, M. Grätzel, J.-E. Moser, *Nat. Photonics* **2014**, *8*, 250; c) S. Panigrahi, S. Jana, T. Calmeiro, D. Nunes, R. Martins, E. Fortunato, *ACS Nano* **2017**, *11*, 10214.
[22] X. Hu, X.-F. Jiang, X. Xing, L. Nian, X. Liu, R. Huang, K. Wang, H.-L. Yip, G. Zhou, *Sol. RRL* **2018**, *2*, 1800083.
[23] Q. Xue, M. Liu, Z. Li, L. Yan, Z. Hu, J. Zhou, W. Li, X.-F. Jiang, B. Xu, F. Huang, Y. Li, H.-L. Yip, Y. Cao, *Adv. Funct. Mater.* **2018**, *28*, 1707444.
[24] Y. Shao, Y. Yuan, J. Huang, *Nat. Energy* **2016**, *1*, 15001.
[25] J. Duan, Y. Zhao, X. Yang, Y. Wang, B. He, Q. Tang, *Adv. Energy Mater.* **2018**, *8*, 1802346.
[26] J. Yuan, X. Ling, D. Yang, F. Li, S. Zhou, J. Shi, Y. Qian, J. Hu, Y. Sun, Y. Yang, X. Gao, S. Duhm, Q. Zhang, W. Ma, *Joule* **2018**, *2*, 2450.
[27] Q. Jiang, Y. Zhao, X. Zhang, X. Yang, Y. Chen, Z. Chu, Q. Ye, X. Li, Z. Yin, J. You, *Nat. Photonics* **2019**, *13*, 460.
[28] J. Kang, L. W. Wang, *J. Phys. Chem. Lett.* **2017**, *8*, 489.
[29] R. E. Brandt, J. R. Poindexter, P. Gorai, R. C. Kurchin, R. L. Z. Hoye, L. Nienhaus, M. W. B. Wilson, J. A. Polizzotti, R. Sereika, R. Žaltauskas, L. C. Lee, J. L. MacManus-Driscoll, M. Bawendi, V. Stevanović, T. Buonassisi, *Chem. Mater.* **2017**, *29*, 4667.
[30] H. Uratani, K. Yamashita, *J. Phys. Chem. Lett.* **2017**, *8*, 742.
[31] D. Meggiolaro, S. G. Motti, E. Mosconi, A. J. Barker, J. Ball, C. Andrea Riccardo Perini, F. Deschler, A. Petrozza, F. De Angelis, *Energy Environ. Sci.* **2018**, *11*, 702.
[32] S. Zhang, S. Wu, W. Chen, H. Zhu, Z. Xiong, Z. Yang, C. Chen, R. Chen, L. Han, W. Chen, *Mater. Today Energy* **2018**, *8*, 125.
[33] L. Zhang, B. Li, J. Yuan, M. Wang, T. Shen, F. Huang, W. Wen, G. Cao, J. Tian, *J. Phys. Chem. Lett.* **2018**, *9*, 3646.
[34] B. Yu, H. Zhang, J. Wu, Y. Li, H. Li, Y. Li, J. Shi, H. Wu, D. Li, Y. Luo, Q. Meng, *J. Mater. Chem. A* **2018**, *6*, 19810.
[35] G. Yin, H. Zhao, H. Jiang, S. Yuan, T. Niu, K. Zhao, Z. Liu, S. F. Liu, *Adv. Funct. Mater.* **2018**, *28*, 1803269.
[36] D. Bai, H. Bian, Z. Jin, H. Wang, L. Meng, Q. Wang, S. Liu, *Nano Energy* **2018**, *52*, 408.
[37] a) N. J. Jeon, J. H. Noh, Y. C. Kim, W. S. Yang, S. Ryu, S. I. Seok, *Nat. Mater.* **2014**, *13*, 897; b) B. Xia, Z. Wu, H. Dong, J. Xi, W. Wu, T. Lei, K. Xi, F. Yuan, B. Jiao, L. Xiao, Q. Gong, X. Hou, *J. Mater. Chem. A* **2016**, *4*, 6295; c) M. Xiao, F. Huang, W. Huang, Y. Dkhissi, Y. Zhu, J. Etheridge, A. Gray-Weale, U. Bach, Y. B. Cheng, L. Spiccia, *Angew. Chem., Int. Ed.* **2014**, *53*, 9898.
[38] C. Dong, X. Han, Y. Zhao, J. Li, L. Chang, W. Zhao, *Sol. RRL* **2018**, *2*, 1800139.
[39] Q. Zhang, W. Zhu, D. Chen, Z. Zhang, Z. Lin, J. Chang, J. Zhang, C. Zhang, Y. Hao, *ACS Appl. Mater. Interfaces* **2019**, *11*, 2997.
[40] J. Lu, S.-C. Chen, Q. Zheng, *ACS Appl. Energy Mater.* **2018**, *1*, 5872.
[41] T. Zhang, M. I. Dar, G. Li, F. Xu, N. Guo, M. Gratzel, Y. Zhao, *Sci. Adv.* **2017**, *3*, e1700841.
[42] U. Khan, Y. Zhinong, A. A. Khan, A. Zulfiqar, N. Ullah, *Nanoscale Res. Lett.* **2019**, *14*, 116.
[43] Y. Hu, S. Zhang, T. Shu, T. Qiu, F. Bai, W. Ruan, F. Xu, *J. Mater. Chem. A* **2018**, *6*, 20365.
[44] J. Liang, P. Zhao, C. Wang, Y. Wang, Y. Hu, G. Zhu, L. Ma, J. Liu, Z. Jin, *J. Am. Chem. Soc.* **2017**, *139*, 14009.
[45] N. Li, Z. Zhu, J. Li, A. K. Y. Jen, L. Wang, *Adv. Energy Mater.* **2018**, *8*, 1800525.
[46] Q. A. Akkerman, G. Raino, M. V. Kovalenko, L. Manna, *Nat. Mater.* **2018**, *17*, 394.
[47] R. E. Brandt, V. Stevanovic, D. S. Ginley, T. Buonassisi, *MRS Commun.* **2015**, *5*, 265.
[48] a) A. Buin, P. Pietsch, J. Xu, O. Voznyy, A. H. Ip, R. Comin, E. H. Sargent, *Nano Lett.* **2014**, *14*, 6281; b) W.-J. Yin, T. Shi, Y. Yan, *Appl. Phys. Lett.* **2014**, *104*, 063903.
[49] F. Yang, D. Hirotani, D. G. Kapil, D. M. A. Kamarudin, D. C. H. Ng, D. Y. Zhang, P. D. Q. Shen, P. D. S. Hayase, *Angew. Chem., Int. Ed.* **2018**, *57*, 12745.
[50] W. Xiang, Z. Wang, D. J. Kubicki, W. Tress, J. Luo, D. Prochowicz, S. Akin, L. Emsley, J. Zhou, G. Dietler, M. Grätzel, A. Hagfeldt, *Joule* **2019**, *3*, 205.
[51] D. Bai, J. Zhang, Z. Jin, H. Bian, K. Wang, H. Wang, L. Liang, Q. Wang, S. F. Liu, *ACS Energy Lett.* **2018**, *3*, 970.
[52] B. Li, Y. Zhang, L. Fu, T. Yu, S. Zhou, L. Zhang, L. Yin, *Nat. Commun.* **2018**, *9*, 1076.
[53] Z. Zeng, J. Zhang, X. Gan, H. Sun, M. Shang, D. Hou, C. Lu, R. Chen, Y. Zhu, L. Han, *Adv. Energy Mater.* **2018**, *8*, 1801050.
[54] Y. Wang, T. Zhang, M. Kan, Y. Li, T. Wang, Y. Zhao, *Joule* **2018**, *2*, 2065.
[55] J. Yuan, L. Zhang, C. Bi, M. Wang, J. Tian, *Sol. RRL* **2018**, *2*, 1800188.
[56] Q. Zeng, X. Zhang, X. Feng, S. Lu, Z. Chen, X. Yong, S. A. T. Redfern, H. Wei, H. Wang, H. Shen, W. Zhang, W. Zheng, H. Zhang, J. S. Tse, B. Yang, *Adv. Mater.* **2018**, *30*, 1705393.
[57] a) F. Fu, S. Pisoni, T. P. Weiss, T. Feurer, A. Wackerlin, P. Fuchs, S. Nishiwaki, L. Zortea, A. N. Tiwari, S. Buecheler, *Adv. Sci.* **2018**, *5*, 1700675; b) W.-H. Lee, C.-Y. Chen, C.-S. Li, S.-Y. Hsiao, W.-L. Tsai, M.-J. Huang, C.-H. Cheng, C.-I. Wu, H.-W. Lin, *Nano Energy* **2017**, *38*, 66; c) B. Li, Y. Zhang, L. Zhang, L. Yin, *Adv. Mater.* **2017**, *29*, 1701221; d) Y. Wu, X. Yang, W. Chen, Y. Yue, M. Cai, F. Xie, E. Bi, A. Islam, L. Han, *Nat. Energy* **2016**, *1*, 16148.
[58] L. Yan, Q. Xue, M. Liu, Z. Zhu, J. Tian, Z. Li, Z. Chen, Z. Chen, H. Yan, H. L. Yip, Y. Cao, *Adv. Mater.* **2018**, *30*, 1802509.
[59] S. Berweger, G. A. MacDonald, M. Yang, K. J. Coakley, J. J. Berry, K. Zhu, F. W. DelRio, T. M. Wallis, P. Kabos, *Nano Lett.* **2017**, *17*, 1796.
[60] a) Y. Bai, S. Xiao, C. Hu, T. Zhang, X. Meng, H. Lin, Y. Yang, S. Yang, *Adv. Energy Mater.* **2017**, *7*, 1701038; b) C. H. Chuang, P. R. Brown, V. Bulovic, M. G. Bawendi, *Nat. Mater.* **2014**, *13*, 796.
[61] J. Zhang, D. Bai, Z. Jin, H. Bian, K. Wang, J. Sun, Q. Wang, S. F. Liu, *Adv. Energy Mater.* **2018**, *8*, 1703246.
[62] L. Liu, A. Mei, T. Liu, P. Jiang, Y. Sheng, L. Zhang, H. Han, *J. Am. Chem. Soc.* **2015**, *137*, 1790.
[63] J. Zhang, Z. Jin, L. Liang, H. Wang, D. Bai, H. Bian, K. Wang, Q. Wang, N. Yuan, J. Ding, S. F. Liu, *Adv. Sci.* **2018**, *5*, 1801123.
[64] G. Liao, J. Duan, Y. Zhao, Q. Tang, *Sol. Energy* **2018**, *171*, 279.
[65] H. Xu, J. Duan, Y. Zhao, Z. Jiao, B. He, Q. Tang, *J. Power Sources* **2018**, *399*, 76.
[66] Q. Li, J. Bai, T. Zhang, C. Nie, J. Duan, Q. Tang, *Chem. Commun.* **2018**, *54*, 9575.
[67] H. Bian, D. Bai, Z. Jin, K. Wang, L. Liang, H. Wang, J. Zhang, Q. Wang, S. Liu, *Joule* **2018**, *2*, 1500.
[68] C. Liu, W. Li, C. Zhang, Y. Ma, J. Fan, Y. Mai, *J. Am. Chem. Soc.* **2018**, *140*, 3825.
[69] C. L. Kennedy, A. H. Hill, E. S. Massaro, E. M. Grumstrup, *ACS Energy Lett.* **2017**, *2*, 1501.
[70] J. S. Manser, P. V. Kamat, *Nat. Photonics* **2014**, *8*, 737.

[71] A. H. Hill, K. E. Smyser, C. L. Kennedy, E. S. Massaro, E. M. Grumstrup, *J. Phys. Chem. Lett.* **2017**, *8*, 948.
[72] S. Christodoulou, F. Di Stasio, S. Pradhan, A. Stavrinadis, G. Konstantatos, *J. Phys. Chem. C* **2018**, *122*, 7621.
[73] F. Liu, C. Ding, Y. Zhang, T. Kamisaka, Q. Zhao, J. M. Luther, T. Toyoda, S. Hayase, T. Minemoto, K. Yoshino, B. Zhang, S. Dai, J. Jiang, S. Tao, Q. Shen, *Chem. Mater.* **2019**, *31*, 798.
[74] Q. A. Akkerman, M. Gandini, F. Di Stasio, P. Rastogi, F. Palazon, G. Bertoni, J. M. Ball, M. Prato, A. Petrozza, L. Manna, *Nat. Energy* **2017**, *2*, 16194.
[75] Erin M. Sanehira, Ashley R. Marshall, Jeffrey A. Christians, Steven P. Harvey, Peter N. Ciesielski, Lance M. Wheeler, Philip Schulz, Lih Y. Lin, M. C. Beard, J. M. Luther, *Sci. Adv.* **2017**, *3*, eaao4204.
[76] a) V. Kapoor, A. Bashir, L. J. Haur, A. Bruno, S. Shukla, A. Priyadarshi, N. Mathews, S. Mhaisalkar, *Energy Technol.* **2017**, *5*, 1880; b) S. Chen, X. Wen, J. S. Yun, S. Huang, M. Green, N. J. Jeon, W. S. Yang, J. H. Noh, J. Seo, S. I. Seok, A. Ho-Baillie, *ACS Appl. Mater. Interfaces* **2017**, *9*, 6072; c) T. J. Jacobsson, J. P. Correa-Baena, E. Halvani Anaraki, B. Philippe, S. D. Stranks, M. E. Bouduban, W. Tress, K. Schenk, J. Teuscher, J. E. Moser, H. Rensmo, A. Hagfeldt, *J. Am. Chem. Soc.* **2016**, *138*, 10331; d) B. W. Park, N. Kedem, M. Kulbak, D. Y. Lee, W. S. Yang, N. J. Jeon, J. Seo, G. Kim, K. J. Kim, T. J. Shin, G. Hodes, D. Cahen, S. I. Seok, *Nat. Commun.* **2018**, *9*, 3301; e) L. Wang, C. McCleese, A. Kovalsky, Y. Zhao, C. Burda, *J. Am. Chem. Soc.* **2014**, *136*, 12205.
[77] Y. Fu, M. T. Rea, J. Chen, D. J. Morrow, M. P. Hautzinger, Y. Zhao, D. Pan, L. H. Manger, J. C. Wright, R. H. Goldsmith, S. Jin, *Chem. Mater.* **2017**, *29*, 8385.
[78] E. M. Hutter, R. J. Sutton, S. Chandrashekar, M. Abdi-Jalebi, S. D. Stranks, H. J. Snaith, T. J. Savenije, *ACS Energy Lett.* **2017**, *2*, 1901.
[79] Q. Wang, Z. Jin, D. Chen, D. Bai, H. Bian, J. Sun, G. Zhu, G. Wang, S. F. Liu, *Adv. Energy Mater.* **2018**, *8*, 1800007.
[80] P. Luo, W. Xia, S. Zhou, L. Sun, J. Cheng, C. Xu, Y. Lu, *J. Phys. Chem. Lett.* **2016**, *7*, 3603.
[81] L. A. Frolova, D. V. Anokhin, A. A. Piryazev, S. Y. Luchkin, N. N. Dremova, K. J. Stevenson, P. A. Troshin, *J. Phys. Chem. Lett.* **2017**, *8*, 67.
[82] S. Xiang, Z. Fu, W. Li, Y. Wei, J. Liu, H. Liu, L. Zhu, R. Zhang, H. Chen, *ACS Energy Lett.* **2018**, *3*, 1824.
[83] B. Zhao, S. F. Jin, S. Huang, N. Liu, J. Y. Ma, D. J. Xue, Q. Han, J. Ding, Q. Q. Ge, Y. Feng, J. S. Hu, *J. Am. Chem. Soc.* **2018**, *140*, 11716.
[84] K. Wang, Z. Jin, L. Liang, H. Bian, D. Bai, H. Wang, J. Zhang, Q. Wang, S. Liu, *Nat. Commun.* **2018**, *9*, 4544.
[85] K. Wang, Z. Jin, L. Liang, H. Bian, H. Wang, J. Feng, Q. Wang, S. Liu, *Nano Energy* **2019**, *58*, 175.
[86] Q. Wang, X. Zheng, Y. Deng, J. Zhao, Z. Chen, J. Huang, *Joule* **2017**, *1*, 371.
[87] X. Ding, H. Chen, Y. Wu, S. Ma, S. Dai, S. Yang, J. Zhu, *J. Mater. Chem. A* **2018**, *6*, 18258.
[88] F. Liu, C. Ding, Y. Zhang, T. S. Ripolles, T. Kamisaka, T. Toyoda, S. Hayase, T. Minemoto, K. Yoshino, S. Dai, M. Yanagida, H. Noguchi, Q. Shen, *J. Am. Chem. Soc.* **2017**, *139*, 16708.
[89] C. F. J. Lau, X. Deng, J. Zheng, J. Kim, Z. Zhang, M. Zhang, J. Bing, B. Wilkinson, L. Hu, R. Patterson, S. Huang, A. Ho-Baillie, *J. Mater. Chem. A* **2018**, *6*, 5580.
[90] S. Xiang, W. Li, Y. Wei, J. Liu, H. Liu, L. Zhu, H. Chen, *Nanoscale* **2018**, *10*, 9996.
[91] A. K. Jena, A. Kulkarni, Y. Sanehira, M. Ikegami, T. Miyasaka, *Chem. Mater.* **2018**, *30*, 6668.
[92] H. Bian, Q. Wang, S. Yang, C. Yan, H. Wang, L. Liang, Z. Jin, G. Wang, S. Liu, *J. Mater. Chem. A* **2019**, *7*, 5740.
[93] T. S. Ripolles, K. Nishinaka, Y. Ogomi, Y. Miyata, S. Hayase, *Sol. Energy Mater. Sol. Cells* **2016**, *144*, 532.
[94] F. Haque, M. Wright, M. A. Mahmud, H. Yi, D. Wang, L. Duan, C. Xu, M. B. Upama, A. Uddin, *ACS Omega* **2018**, *3*, 11937.
[95] M. Shahiduzzaman, K. Yonezawa, K. Yamamoto, T. S. Ripolles, M. Karakawa, T. Kuwabara, K. Takahashi, S. Hayase, T. Taima, *ACS Omega* **2017**, *2*, 4464.
[96] K. Yonezawa, K. Yamamoto, M. Shahiduzzaman, Y. Furumoto, K. Hamada, T. S. Ripolles, M. Karakawa, T. Kuwabara, K. Takahashi, S. Hayase, T. Taima, *Jpn. J. Appl. Phys.* **2017**, *56*, 04CS11.
[97] H. Choi, J. Jeong, H.-B. Kim, S. Kim, B. Walker, G.-H. Kim, J. Y. Kim, *Nano Energy* **2014**, *7*, 80.
[98] C. Y. Chen, H. Y. Lin, K. M. Chiang, W. L. Tsai, Y. C. Huang, C. S. Tsao, H. W. Lin, *Adv. Mater.* **2017**, *29*, 1605290.
[99] L. M. Wheeler, E. M. Sanehira, A. R. Marshall, P. Schulz, M. Suri, N. C. Anderson, J. A. Christians, D. Nordlund, D. Sokaras, T. Kroll, S. P. Harvey, J. J. Berry, L. Y. Lin, J. M. Luther, *J. Am. Chem. Soc.* **2018**, *140*, 10504.
[100] D. Ghosh, M. Y. Ali, D. K. Chaudhary, S. Bhattacharyya, *Sol. Energy Mater. Sol. Cells* **2018**, *185*, 28.
[101] X. Ling, S. Zhou, J. Yuan, J. Shi, Y. Qian, B. W. Larson, Q. Zhao, C. Qin, F. Li, G. Shi, C. Stewart, J. Hu, X. Zhang, J. M. Luther, S. Duhm, W. Ma, *Adv. Energy Mater.* **2019**, *9*, 1900721.
[102] K. Chen, Q. Zhong, W. Chen, B. Sang, Y. Wang, T. Yang, Y. Liu, Y. Zhang, H. Zhang, *Adv. Funct. Mater.* **2019**, *29*, 1900991.
[103] J. K. Nam, M. S. Jung, S. U. Chai, Y. J. Choi, D. Kim, J. H. Park, *J. Phys. Chem. Lett.* **2017**, *8*, 2936.
[104] H. Wang, H. Bian, Z. Jin, L. Liang, D. Bai, Q. Wang, S. F. Liu, *Sol. RRL* **2018**, *2*, 1800216.
[105] M. Tai, G. Wang, X. Yin, Y. Zhou, J. Han, Y. Wei, K. Jiang, H. Lin, *Energy Technol.* **2019**, *7*, 1800986.
[106] J. K. Nam, S. U. Chai, W. Cha, Y. J. Choi, W. Kim, M. S. Jung, J. Kwon, D. Kim, J. H. Park, *Nano Lett.* **2017**, *17*, 2028.
[107] S. Mariotti, O. S. Hutter, L. J. Phillips, P. J. Yates, B. Kundu, K. Durose, *ACS Appl. Mater. Interfaces* **2018**, *10*, 3750.
[108] Y. Li, Y. Wang, T. Zhang, S. Yoriya, P. Kumnorkaew, S. Chen, X. Guo, Y. Zhao, *Chem. Commun.* **2018**, *54*, 9809.
[109] Y. Gao, Y. Dong, K. Huang, C. Zhang, B. Liu, S. Wang, J. Shi, H. Xie, H. Huang, S. Xiao, J. He, Y. Gao, R. A. Hatton, J. Yang, *ACS Photonics* **2018**, *5*, 4104.
[110] J. S. Niezgoda, B. J. Foley, A. Z. Chen, J. J. Choi, *ACS Energy Lett.* **2017**, *2*, 1043.
[111] R. J. Sutton, G. E. Eperon, L. Miranda, E. S. Parrott, B. A. Kamino, J. B. Patel, M. T. Hörantner, M. B. Johnston, A. A. Haghighirad, D. T. Moore, H. J. Snaith, *Adv. Energy Mater.* **2016**, *6*, 1502458.
[112] Q. Ma, S. Huang, S. Chen, M. Zhang, C. F. J. Lau, M. N. Lockrey, H. K. Mulmudi, Y. Shan, J. Yao, J. Zheng, X. Deng, K. Catchpole, M. A. Green, A. W. Y. Ho-Baillie, *J. Phys. Chem. C* **2017**, *121*, 19642.
[113] C. F. J. Lau, M. Zhang, X. Deng, J. Zheng, J. Bing, Q. Ma, J. Kim, L. Hu, M. A. Green, S. Huang, A. Ho-Baillie, *ACS Energy Lett.* **2017**, *2*, 2319.
[114] L. Fu, Y. Zhang, B. Chang, B. Li, S. Zhou, L. Zhang, L. Yin, *J. Mater. Chem. A* **2018**, *6*, 13263.
[115] Y. Wang, T. Zhang, F. Xu, Y. Li, Y. Zhao, *Sol. RRL* **2018**, *2*, 1700180.
[116] H. Rao, S. Ye, F. Gu, Z. Zhao, Z. Liu, Z. Bian, C. Huang, *Adv. Energy Mater.* **2018**, *8*, 1800758.
[117] H. Jiang, J. Feng, H. Zhao, G. Li, G. Yin, Y. Han, F. Yan, Z. Liu, S. F. Liu, *Adv. Sci.* **2018**, *5*, 1801117.
[118] H. Zai, D. Zhang, L. Li, C. Zhu, S. Ma, Y. Zhao, Z. Zhao, C. Chen, H. Zhou, Y. Li, Q. Chen, *J. Mater. Chem. A* **2018**, *6*, 23602.
[119] R. E. Beal, D. J. Slotcavage, T. Leijtens, A. R. Bowring, R. A. Belisle, W. H. Nguyen, G. F. Burkhard, E. T. Hoke, M. D. McGehee, *J. Phys. Chem. Lett.* **2016**, *7*, 746.
[120] S. S. Mali, J. V. Patil, C. K. Hong, *Nano Lett.* **2019**, *19*, 6213.
[121] K. L. Wang, R. Wang, Z. K. Wang, M. Li, Y. Zhang, H. Ma, L. S. Liao, Y. Yang, *Nano Lett.* **2019**, *19*, 5176.

[122] Y. Zhang, C. Wu, D. Wang, Z. Zhang, X. Qi, N. Zhu, G. Liu, X. Li, H. Hu, Z. Chen, L. Xiao, B. Qu, *Sol. RRL* **2019**, https://doi.org/10.1002/solr.201900254.

[123] J. Liang, Z. Liu, L. Qiu, Z. Hawash, L. Meng, Z. Wu, Y. Jiang, L. K. Ono, Y. Qi, *Adv. Energy Mater.* **2018**, *8*, 1800504.

[124] B. Yang, M. Wang, X. Hu, T. Zhou, Z. Zang, *Nano Energy* **2019**, *57*, 718.

[125] W. Li, M. U. Rothmann, A. Liu, Z. Wang, Y. Zhang, A. R. Pascoe, J. Lu, L. Jiang, Y. Chen, F. Huang, Y. Peng, Q. Bao, J. Etheridge, U. Bach, Y.-B. Cheng, *Adv. Energy Mater.* **2017**, *7*, 1700946.

[126] Q. Ma, S. Huang, X. Wen, M. A. Green, A. W. Y. Ho-Baillie, *Adv. Energy Mater.* **2016**, *6*, 1502202.

[127] C. F. J. Lau, X. Deng, Q. Ma, J. Zheng, J. S. Yun, M. A. Green, S. Huang, A. W. Y. Ho-Baillie, *ACS Energy Lett.* **2016**, *1*, 573.

[128] C. Liu, W. Li, J. Chen, J. Fan, Y. Mai, R. E. I. Schropp, *Nano Energy* **2017**, *41*, 75.

[129] W. Zhu, Q. Zhang, D. Chen, Z. Zhang, Z. Lin, J. Chang, J. Zhang, C. Zhang, Y. Hao, *Adv. Energy Mater.* **2018**, *8*, 1802080.

[130] J. Lin, M. Lai, L. Dou, C. S. Kley, H. Chen, F. Peng, J. Sun, D. Lu, S. A. Hawks, C. Xie, F. Cui, A. P. Alivisatos, D. T. Limmer, P. Yang, *Nat. Mater.* **2018**, *17*, 261.

[131] Y. Guo, X. Yin, J. Liu, W. Que, *J. Mater. Chem. A* **2019**, *7*, 19008.

[132] S. Sanchez, N. Christoph, B. Grobety, N. Phung, U. Steiner, M. Saliba, A. Abate, *Adv. Energy Mater.* **2018**, *8*, 1802060.

[133] Z. Li, J. Xu, S. Zhou, B. Zhang, X. Liu, S. Dai, J. Yao, *ACS Appl. Mater. Interfaces* **2018**, *10*, 38183.

[134] M. Kulbak, D. Cahen, G. Hodes, *J. Phys. Chem. Lett.* **2015**, *6*, 2452.

[135] M. Kulbak, S. Gupta, N. Kedem, I. Levine, T. Bendikov, G. Hodes, D. Cahen, *J. Phys. Chem. Lett.* **2016**, *7*, 167.

[136] J. Duan, Y. Zhao, B. He, Q. Tang, *Angew. Chem., Int. Ed.* **2018**, *57*, 3787.

[137] Y. Li, J. Duan, H. Yuan, Y. Zhao, B. He, Q. Tang, *Sol. RRL* **2018**, *2*, 1800164.

[138] X. Zhang, Z. Jin, J. Zhang, D. Bai, H. Bian, K. Wang, J. Sun, Q. Wang, S. F. Liu, *ACS Appl. Mater. Interfaces* **2018**, *10*, 7145.

[139] J. Lei, F. Gao, H. Wang, J. Li, J. Jiang, X. Wu, R. Gao, Z. Yang, S. Liu, *Sol. Energy Mater. Sol. Cells* **2018**, *187*, 1.

[140] X. Chang, W. Li, L. Zhu, H. Liu, H. Geng, S. Xiang, J. Liu, H. Chen, *ACS Appl. Mater. Interfaces* **2016**, *8*, 33649.

[141] J. B. Hoffman, G. Zaiats, I. Wappes, P. V. Kamat, *Chem. Mater.* **2017**, *29*, 9767.

[142] J. Duan, D. Dou, Y. Zhao, Y. Wang, X. Yang, H. Yuan, B. He, Q. Tang, *Mater. Today Energy* **2018**, *10*, 146.

[143] J. Liang, C. Wang, Y. Wang, Z. Xu, Z. Lu, Y. Ma, H. Zhu, Y. Hu, C. Xiao, X. Yi, G. Zhu, H. Lv, L. Ma, T. Chen, Z. Tie, Z. Jin, J. Liu, *J. Am. Chem. Soc.* **2016**, *138*, 15829.

[144] B. Li, Y. Zhang, L. Zhang, L. Yin, *J. Power Sources* **2017**, *360*, 11.

[145] J. Duan, T. Hu, Y. Zhao, B. He, Q. Tang, *Angew. Chem., Int. Ed.* **2018**, *57*, 5746.

[146] S. Y. Luchkin, A. F. Akbulatov, L. A. Frolova, S. A. Tsarev, P. A. Troshin, K. J. Stevenson, *Sol. Energy Mater. Sol. Cells* **2017**, *171*, 205.

[147] H. Li, G. Tong, T. Chen, H. Zhu, G. Li, Y. Chang, L. Wang, Y. Jiang, *J. Mater. Chem. A* **2018**, *6*, 14255.

[148] W. Chen, J. Zhang, G. Xu, R. Xue, Y. Li, Y. Zhou, J. Hou, Y. Li, *Adv. Mater.* **2018**, *30*, 1800855.